



**SYNTHESIS AND CHARACTERIZATION OF TiO₂ NANOTUBES
FOR DYE-SENSITIZED SOLAR CELLS**

BUAGUN SAMRAN

**A THESIS SUBMITTED IN PARTIAL FULFILLMENT OF THE REQUIREMENTS
FOR THE DEGREE OF DOCTOR OF PHILOSOPHY
MAJOR IN PHYSICS
FACULTY OF SCIENCE
UBON RATCHATHANI UNIVERSITY
YEAR 2013
COPYRIGHT OF UBON RATCHATHANI UNIVERSITY**



THESIS APPROVAL
UBON RATCHATHANI UNIVERSITY
DOCTOR OF PHILOSOPHY
MAJOR IN PHYSICS FACULTY OF SCIENCE

TITLE SYNTHESIS AND CHARACTERIZATION OF TiO_2 NANOTUBES FOR
DYE-SENSITIZED SOLAR CELLS

NAME MR.BUAGUN SAMRAN

THIS THESIS HAS BEEN ACCEPTED BY

..... *Ue. Tippach* CHAIR
(ASST.PROF.DR.UDOM TIPPARACH)
..... *Supakorn Pukird* COMMITTEE
(ASSOC.PROF.DR.SUPAKORN PUKIRD)
..... *Christian HB* COMMITTEE
(DR.CHRISTIAN HERBST)
..... *P. Krongkitsiri* COMMITTEE
(DR.PACHAREE KRONGKITSIRI)

..... *Jan -* DEAN
(ASST.PROF.DR.JANPEN INTARAPRASERT)

APPROVAL BY UBON RATCHATHANI UNIVERSITY

..... *Utith Inprasit*
(ASSOC.PROF.DR.UTITH INPRASIT)
VICE PRESIDENT FOR ACADEMIC AFFAIRS
FOR THE PRESIDENT OF UBON RATCHATHANI UNIVERSITY
ACADEMIC YEAR 2013

ACKNOWLEDGEMENTS

It is a pleasure to acknowledge the generous help of the people who have assisted in the research for and preparation of this thesis. I am heartily thankful to my supervisor, Asst.Prof.Dr.Udom Tipparach, whose encouragement, guidance and support from the initial to the final level enabled me to develop an understanding of the subject. Special thank the thesis committee, Assoc.Prof.Dr.Supakorn Pukird and Dr. Christian Herbst for their kindly advices and helpful suggestions. I would like to thank the external committee member, Dr. Pacharee Krongkitsiri from Department of Science and Mathematics, Faculty of Industry and Technology, Rajamangala University of Technology for her comments and suggestions.

In addition, I would like to thank all faculty members in Department of Physics, Faculty of Science, Ubon Ratchathani University for their teaching and technical supports for this work. I would also like to thank Human Resource Development in Science project (Science Achievement Scholarship of Thailand, SAST) for financial supports.

Finally, I thank my parents and my brother for encouragement supports always. I would not be here today without them.

B. Samran
(Mr.Buagun Samran)
Researcher

บทคัดย่อ

ชื่อเรื่อง : การสังเคราะห์และการศึกษาสมบัติบ่งชี้ของท่อนาโนไททาเนียมไดออกไซด์สำหรับผลิตเซลล์แสงอาทิตย์สีย้อมไวแสง

โดย : บัวกัน ตำราญ

ชื่อปริญญา : ปรัชญาคุณวุฒิบัณฑิต

สาขาวิชา : ฟิสิกส์

ประธานกรรมการที่ปรึกษา : ผู้ช่วยศาสตราจารย์ ดร.อุดม ทิพรราช

คำที่สำคัญ : ท่อนาโนไททาเนียมไดออกไซด์ เซลล์แสงอาทิตย์สีย้อมไวแสง อโนไคเซชัน ไททาเนียมออกไซด์

ท่อนาโนไททาเนียมไดออกไซด์ (TiO_2) ในฐานะวัสดุเพื่อการผันพลังงานได้ถูกเตรียมสำหรับผลิตเซลล์แสงอาทิตย์สีย้อมไวแสง วิธีการอโนไคเซชันได้ถูกใช้สังเคราะห์ท่อนาโนไททาเนียมไดออกไซด์ด้วยการใช้บนแผ่นไททาเนียเป็นฐานรอง สารละลายอิเล็กโทรไลต์เป็นชนิดผสมประกอบด้วยเอทาลีนไกลคอล (EG) แอมโมเนียฟลูออไรด์ (0.3%wt NH_4F) และน้ำ (2%V H_2O) แรงดันไฟฟ้ากระแสตรง 50 โวลต์ถูกใช้ อโนไคเซชัน ด้วยความยาวช่วงเวลาอโนไคเซชันที่ต่างกัน 30 นาที 1 2 4 6 และ 12 ชั่วโมงตามลำดับ ตัวอย่างที่ได้จากการการอโนไคเซชันถูกบำบัดความร้อนอุณหภูมิ 450 องศาเซลเซียส 2 ชั่วโมง ท่อนาโนไททาเนียมไดออกไซด์ถูกศึกษาลักษณะเฉพาะโดยเทคนิคการเลี้ยวเบนรังสีเอ็กซ์ (XRD) กล้องจุลทรรศน์อิเล็กตรอนแบบส่องกราด (SEM) และกล้องจุลทรรศน์แบบแรงอะตอม (AFM) ผลการวิจัยพบว่าโครงสร้างของท่อนาโนไททาเนียมไดออกไซด์เป็นอสัณฐานของนาโนไททาเนียมไดออกไซด์ และเปลี่ยนรูปร่างจากอสัณฐานเป็นผลึกอนาเทสเฟสหลังจากการบำบัดความร้อน และลักษณะทางพื้นผิวของท่อนาโนไททาเนียมไดออกไซด์แสดงให้เห็นขนาดของท่อระหว่าง 30–220 นาโนเมตรทุกเงื่อนไข เส้นผ่านศูนย์กลางของท่อนาโนไททาเนียมไดออกไซด์ขนาดเล็กสุดประมาณคือ 30 นาโนเมตรได้จากเวลาการอโนไคเซชัน 30 นาที ประสิทธิภาพการผันพลังงานของเซลล์แสงอาทิตย์สีย้อมไวแสงเพิ่มขึ้นเมื่อเวลาการอโนไคเซชันเพิ่มขึ้น และประสิทธิภาพของเซลล์แสงอาทิตย์สีย้อมไวแสงสูงสุดคือ 7.92 เปอร์เซ็นต์สำหรับเวลาอโนไคเซชัน 12 ชั่วโมง

CONTENTS

| | PAGE |
|---|-------------|
| ACKNOWLEDGMENTS | I |
| THAI ABSTRACT | II |
| ENGLISH ABSTRACT | III |
| CONTENTS | IV |
| LIST OF TABLES | VI |
| LIST OF FIGURES | VII |
| CHAPTER | |
| 1 INTRODUCTION | |
| 1.1 Motivation and background | 1 |
| 1.2 Research Objectives | 2 |
| 1.3 Scope of this work | 3 |
| 2 THEORETICAL AND LITERATURE REVIEWS | |
| 2.1 Structures and properties of TiO ₂ materials | 4 |
| 2.2 Preparation of TiO ₂ nanotubes | 10 |
| 2.3 TiO ₂ nanotubes formation | 15 |
| 2.4 The dye-sensitized solar cells | 20 |
| 2.4.1 Principle of dye-sensitized solar cells | 20 |
| 2.4.2 The efficiency of dye-sensitized solar cells | 22 |
| 3 EXPERIMENTAL | |
| 3.1 Materials and Thin films preparation | 24 |
| 3.2 Anodization method | 25 |
| 3.3 The characterization of TiO ₂ nanotubes | 27 |
| 3.3.1 Scanning Electron Microscopy Analysis (SEM) | 27 |
| 3.3.2 X-ray Diffraction Analysis (XRD) | 28 |
| 3.3.3 Atomic Force Microscope Analysis (AFM) | 31 |
| 3.4 The preparation of dye-sensitized solar cells | 33 |

CONTENTS (CONTINUED)

| | PAGE |
|--|-------------|
| 4 RESULTS AND DISCUSSIONS | |
| 4.1 XRD patterns | 35 |
| 4.2 SEM analysis | 37 |
| 4.3 AFM analysis | 40 |
| 4.4 The efficiencies of dye-sensitized solar cells | 43 |
| 5 CONCLUSIONS AND SUGGESTIONS | 45 |
| REFERENCES | 47 |
| APPENDIX | 54 |
| VITAE | 56 |

LIST OF TABLES

| TABLES | PAGE |
|--|-------------|
| 3.1 Specifications of PSI Ultralevers | 32 |
| 4.1 The efficiencies of dye-sensitized solar cells | 44 |

LIST OF FIGURES (CONTINUED)

| FIGURES | PAGE |
|--|------|
| 3.2 Flowchart of preparation of TiO ₂ nanotubes by anodization method for dye-sensitized solar cells | 26 |
| 3.3 A JEOL JSM-5410 Scanning Electron Microscopy | 27 |
| 3.4 A PHILIPS X'Pert MPD diffractometer using Cu K _α radiation of wavelength of 0.154 nm | 28 |
| 3.5 Schematic of AFM operation | 31 |
| 3.6 Schematic of Van der Waals force as a function of tip-sample distance in non-contact mode AFM | 32 |
| 3.7 TiO ₂ nanotubes were immersed in N719 dye | 33 |
| 3.8 Shows preparation of dye-sensitized solar cells | 34 |
| 3.9 Shows measurement device of IV curves for dye-sensitized solar cells | 34 |
| 4.1 XRD patterns of the TiO ₂ nanotubes as-anodized samples with different anodizing times: 30 min, 1 h, 2 h, 4 h, 6 h and 12 h before annealing | 35 |
| 4.2 XRD patterns of the TiO ₂ nanotubes with different anodizing times: 30 min, 1 h, 2 h, 4 h and 6 h after annealing at 450 °C 2 h | 36 |
| 4.3 SEM images of TiO ₂ nanotube arrays with different anodizing times: (a) 30 min, (b) 1 h, (c) 2 h (d), 4 h (e) 6 h and (f) 12 h | 38 |
| 4.4 AFM images of TiO ₂ nanotubes with different anodizing times: (a) 30 min, (b) 1 h, (c) 2 h, (d) 4 h, (e) 6 h and (f) 12 h | 41 |
| 4.5 I-V characteristic of the dye-sensitized solar cells on the TiO ₂ nanotube arrays with different anodizing times: 30 min, 1 h, 2 h, 4 h, 6 h and 12 h | 43 |

CHAPTER 1

INTRODUCTION

1.1 Motivation and background

Worldwide energy problems are increase of energy consumption that result in decreasing of non-sustainable fossil fuels such as oil, natural gas, coal [1] and emission of global green-house gases such as carbon dioxide and carbon monoxide. So, the development of renewable energy is a key concern. Solar cells are widely considered to be the future of renewable energy and as one of the competitive alternatives to fossil fuel - based energy sources [2]. The dye sensitized solar cell is one of the most promising ways to realize solar cell economy for the following reasons: this process is based on solar energy, from sunlight which is a clean and everlasting source of energy. Dye-sensitized solar cells are the photovoltaic devices of choice because of their high efficiency, low production cost and easy fabrication [3]. The efficiency of dye sensitized solar cells is 11.2 % with the TiO_2 nanoparticle [4-5]. This efficiency is low for commercialization of dye sensitized solar cells. For application in dye sensitized solar cells, TiO_2 nanotubes have higher charge collection efficiencies than a nanoparticle structure due to their faster transport and slower recombination of electrons [3]. In recent years, TiO_2 nanotubes have attracted more attention due to their excellent physical and chemical properties [6]. They have been widely used in various applications such as solar energy cells [7], photocatalysis [8] and gas sensors [9]. TiO_2 nanotubes have been successfully fabricated by several methods, hydrothermal techniques [10], sol gel transcription [11], seed growth method [12] and electrochemical anodic oxidation. Among these methods, electrochemical anodic oxidation is the simplest and likely the cheapest. However, during the anodization process, preparation parameters influencing the structure of TiO_2 nanotubes have been reported. These various parameters include electrolyte composition, the anodic voltage, time and pH [13]. However, there is little information on the process parameters of TiO_2 nanotubes such as treatment times in anodization in the published papers.

In this work, we proposed to prepare TiO_2 nanotubes by anodization method in mixture electrolytes. We used TiO_2 nanotubes to fabricate dye-sensitized solar cells. Eventually, we performed the measurement of the solar cells efficiency.

1.2 Research objectives

The goals of this thesis are to prepare TiO_2 nanotubes by anodization method for the dye-sensitized solar cells, to study the effects of different extension periods of times anodization, and to measure the conversion efficiency of the dye-sensitized solar cells.

1.3 Scope of this work

TiO₂ nanotubes were produced and were used to fabricate the samples for dye sensitized solar cells. Then, all samples were characterized by using X-ray diffraction (XRD), Atomic Force Microscopy (AFM) and Scanning Electron Microscopy (SEM). TiO₂ nanotubes were used to improve efficiency of dye-sensitized solar cells. The scope of this work is shown in Figure 1.1.

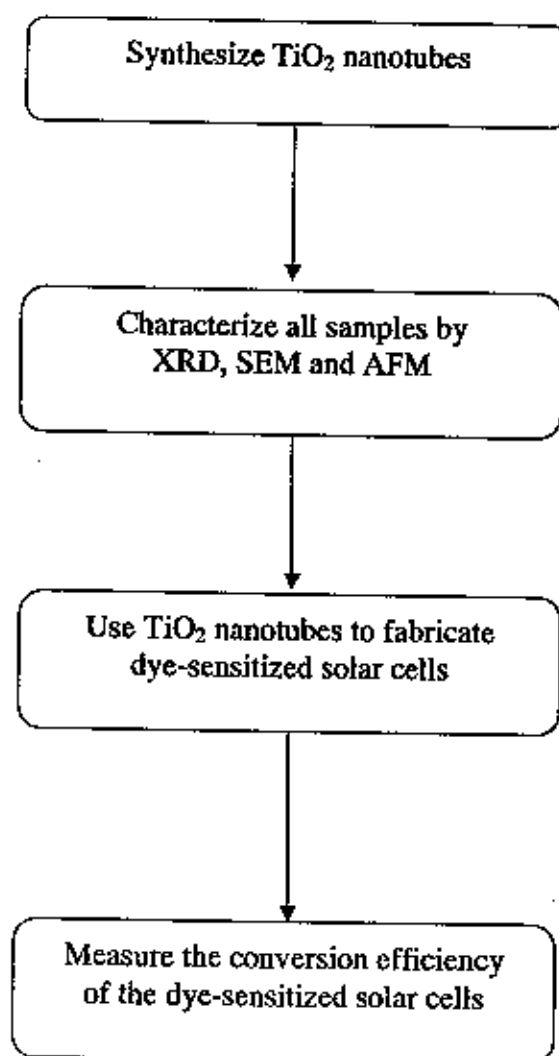


Figure 1.1 Diagram of the scope in this research.

CHAPTER 2

THEORETICAL AND LITERATURE REVIEWS

This chapter contains a review of properties and structures of TiO_2 materials, the anodization process, effect of deposition parameters, the microstructural properties of TiO_2 nanotubes thin films and the concepts of dye-sensitized solar cells. In general, many methods can be used in the preparation of TiO_2 nanotubes thin films such as sol gel [14], hydrothermal process [15] and anodization method [16-17]. The mechanism of TiO_2 nanotubes formation is also presented in this Chapter.

2.1 Structures and properties of TiO_2 materials

Titanium dioxide (TiO_2) or Titania naturally occurs in a form of oxide of titanium. Titanium dioxide occurs in nature as well-known minerals rutile, anatase and brookite. TiO_2 is a cheap and innocuous inorganic material extensively employed in industrial and commercial application such as pigment in the paint industry and as a binder in the medical field. For instance, more than 4 million tones of the white pigment are annually consumed by the paint industry worldwide, being the most widely used pigment because of its brightness, high refractive index and low-cost [18]. TiO_2 is a wide band gap semiconductor that presents photoactivity upon near UV or higher irradiation, absorbing photons and transforming them into chemical redox energy. Although TiO_2 is inert and does not promote chemical reactions without irradiation, the handling of very finely divided TiO_2 particles requires taking safety measures. TiO_2 is rapidly growing worldwide due to its unique electronic properties, combined with the possibility of easy applications in nanostructures. TiO_2 can in fact be manipulated by a wide spectrum of techniques and shaped into a broad range of nanoscale morphologies: particles, wires, rods, tubes and thin films [19]. Titania exists in a number of crystalline forms anatase, rutile and brookite. The most important of phases are anatase and rutile.

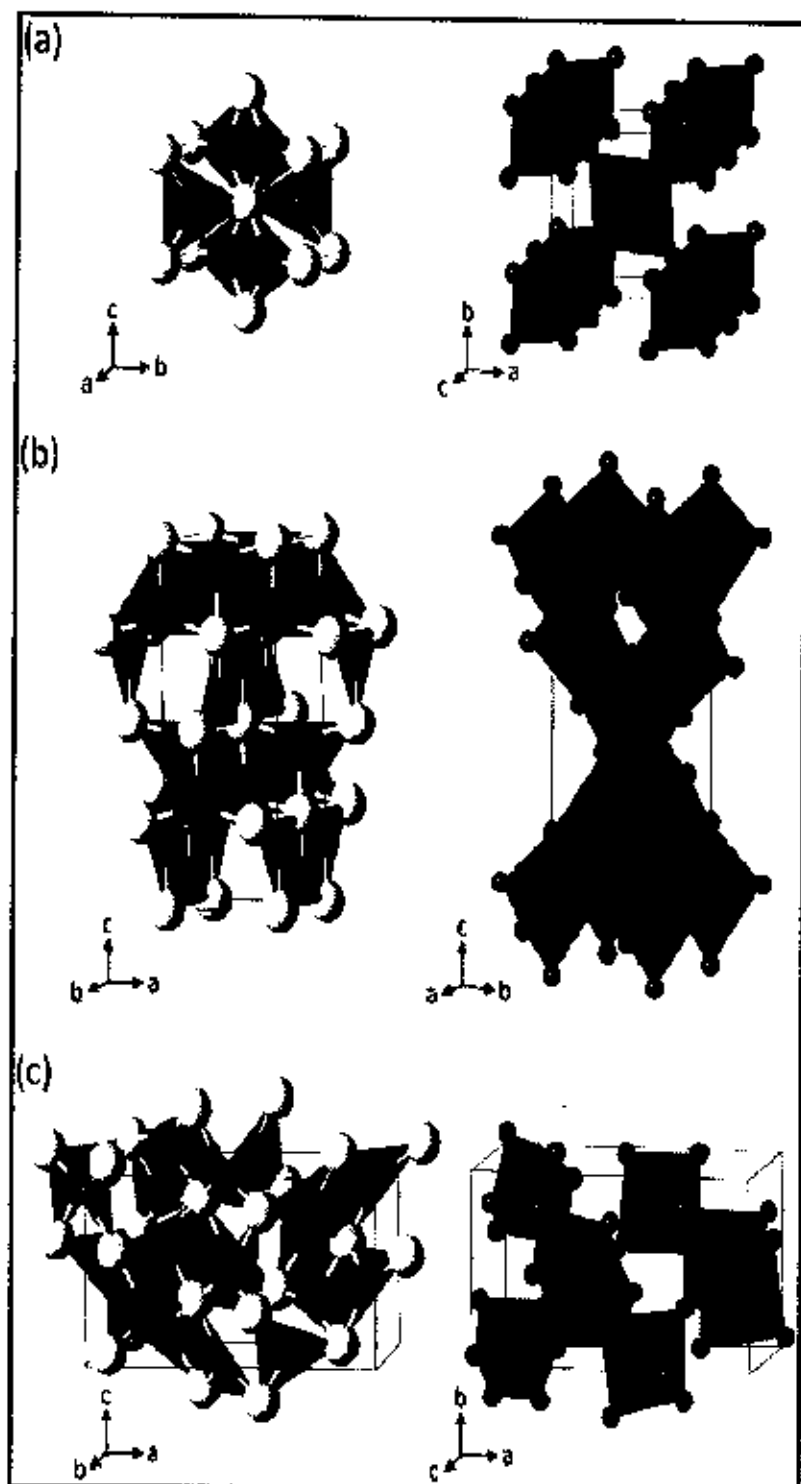


Figure 2.1 A schematic diagram of TiO₂ structure: (a) rutile phase (b) anatase phase and (c) brookite [20].

Anatase, rutile and brookite are the three main crystalline phases of TiO_2 . In this work, we focus on the first and second crystallites because they have an effect on the optical and electronic properties of films serving as photoanodes. Anatase, rutile and brookite phases are shown in Figure 2.1. In titania polymorphs, the basic building blocks consist of a titanium atom surrounded by six oxygen atoms in a more or less distorted TiO_6 octahedral configuration. The crystal structure differs by the distortion of each octahedron and by the assembly patterns of the octahedral chain.

In rutile, neighboring TiO_6 units share corner, being stacked with their long axis alternating by 90° . Anatase framework consists of strongly distorted edge sharing TiO_6 octahedron. Corner sharing and edge sharing octahedral units give rise to the three dimensional network of TiO_2 -B. Differences in mass density and electronic band structure are explained in terms of the different lattice structure. The anatase and TiO_2 -B phases are known to be thermodynamically less stable than the rutile phase so that they are converted into the other phases at high temperature. It is generally accepted that anatase is the most photoactive form of titania [21]. The bulk structure of titania networks is quite complex with various types of intrinsic defects including oxygen vacancies. Such oxygen deficiency implies the presence of some Ti (III) centers that behave like electron-donating species, providing an n-type character to the semiconductor.

The phase change from amorphous to the crystalline anatase and rutile phase occurs with increased temperature or heat treatment, although the anatase and rutile are stable structures at low and high temperatures, respectively. Amorphous anatase can convert to crystalline anatase with heat treatment at approximately 280°C and above. A mixture of anatase and rutile will undergo the conversion at temperatures higher than 430°C . Figure 2.2 indicates formation of nanocrystalline TiO_2 nanotubes after annealing or heat treatment. The exhibition of glancing angle X-ray diffraction pattern of the nanotube arrays samples was annealed at temperatures ranging from 230°C to 880°C in dry oxygen ambient for three hours.

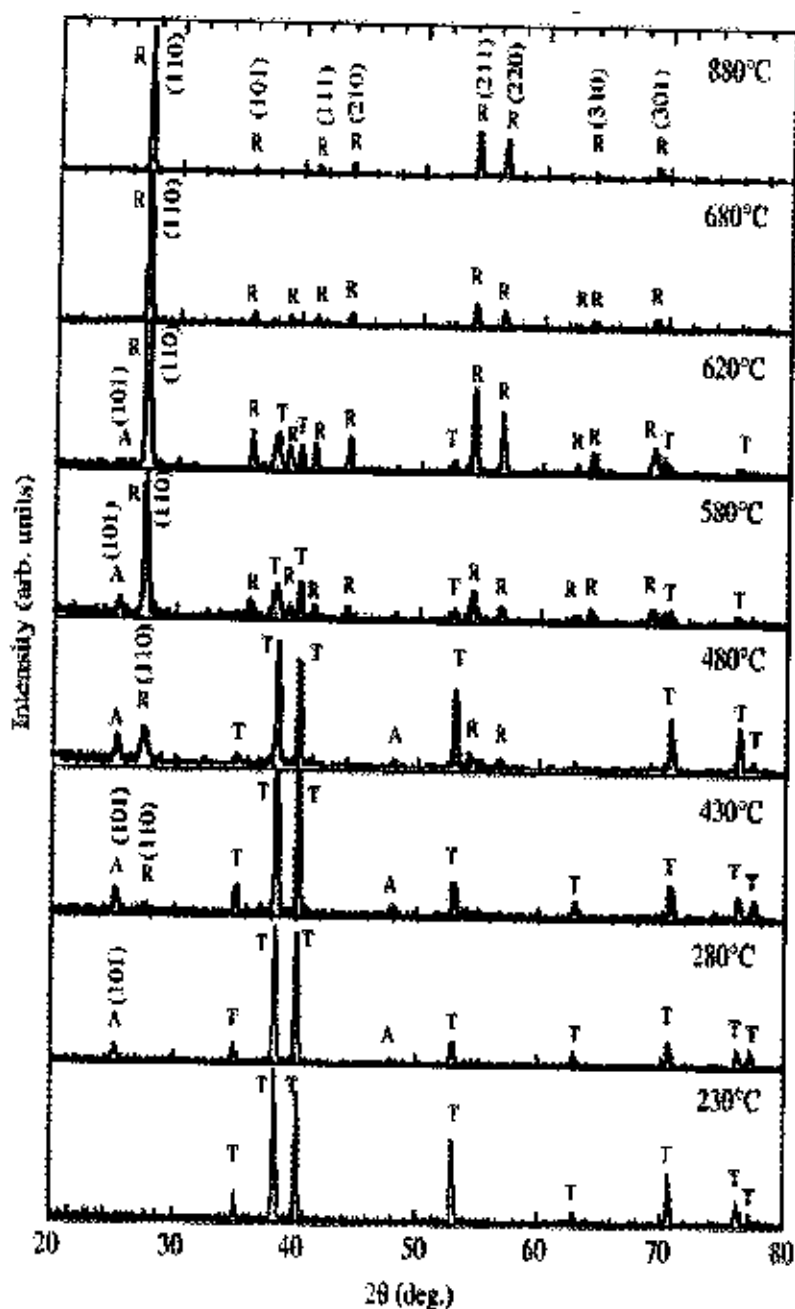


Figure 2.2 Glancing angle X-ray diffraction patterns of the nanotube arrays annealed at temperatures ranging from 230 to 880 °C dry oxygen ambient for three hours. A, R and T represent anatase, rutile and titanium respectively [22].

The properties of semiconductors can be understood by chemical interpretation of the band theory as shown Figure 2.3. According to this theory, at 0 K, a perfect crystal of a semiconductor material possesses a group of very closely filled electronic states (valence band, VB) and another group of closely empty electronic states at higher energies (conduction band, CB). A region where no electronic states are available (band gap) exists between the VB and the CB.

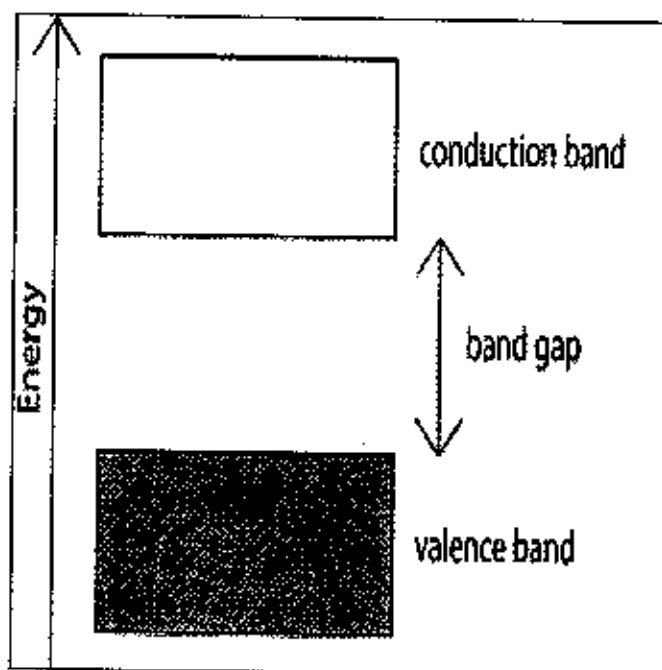


Figure 2.3 A schematic diagram showing the band gap of a semiconductor.

TiO₂ is a wide band gap semiconductor material (3.0-3.2 eV depending on the crystalline phase [23]), capable of converting energy from light into chemical redox energy. If an incident photon of energy greater than or equal to the band gap of the semiconductor is absorbed, an electron from the VB is promoted into the CB leaving a hole behind. The number of photogenerated electron-hole pairs depends on the semiconductor band structure as well as the energy and the effective intensity of the incident light.

Figure 2.4 shows the redox potentials associated to the conduction and valence bands of titania which defines the thermodynamic requirements for interfacial electron transfer reactions. While titania electron conduction band is a moderate reducing agent, hole valence band possesses strong oxidizing power. In order for an electron acceptor A to be spontaneously photoreduced, the potential of the semiconductor must be more positive than the CB reduction potential of the A/A^+ pair. Following a similar reasoning, to assist the oxidation of an electron donor D, the potential of the semiconductor VB must be more positive than the reduction potential of D^+/D pair.

Therefore, assuming no kinetic limitations, light-induced semiconductor assisted interfacial redox reactions will take place with acceptors and electron donors whose respective reduction potentials fall between the CB and VB band positions. Due to TiO_2 inertness, low-cost and low-solubility, it has great potentials for applications as a semiconductor.

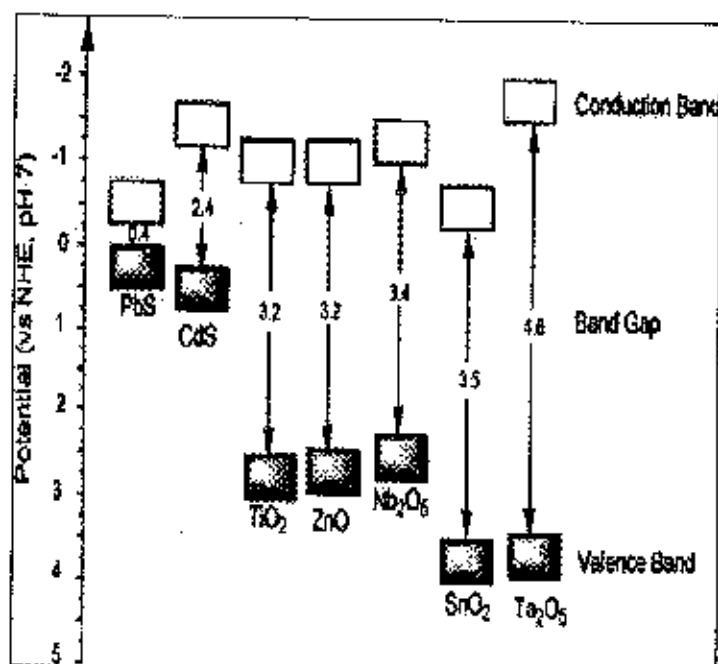


Figure 2.4 A schematic showing the energy gap values of some semiconductor materials [24].

2.2 Preparation of TiO₂ nanotubes

In 1972, Fujishima and Honda began the application of titanium dioxide (TiO₂) in photocatalytic splitting of water [25]. This discovery was a driving force and motivation to thin films creation and development of other materials. Recently, researchers have started to focus on surface modification and bio-implantation in the nanoscale regime because of the natural physiological environment to which bone cells are accustomed. Synthesis of nanostructured titanium dioxide (TiO₂) such as nanotubes, nanowires and nanofibers has raised interest lately due to their high surface to-volume ratio and the ability to provoke a greater degree of biological plasticity, compared to conventional microstructures. Nanostructured TiO₂ has been widely used in various applications such as biosensors [26], solar cells [27], photocatalysis [28], photoelectrolysis [29] and biomaterials [26]. A considerable number of studies have proved that surfaces comprised of nanostructured TiO₂ exhibit positive effect on cell behavior such as significant accelerated rate of apatite formation, enhanced osteoblast adhesion, as well as proliferation and differentiation. Accordingly, these findings strongly suggest the use of nanostructured TiO₂ as a future implant material.

TiO₂ nanotubes can be prepared by anodization method under optimal conditions: pH, voltage, anodization time, electrolyte, cathode and temperature bath. The pH value is also one of the most important factors that affect the length of the tubes [30]. The basic environment pH 8-9 is much more efficient for the formation of longer nanotubes than the commonly used acidic condition. During the formation of nanotubes with 1.8 μm length after 6 h of anodization in aqueous electrolyte with pH 4-5, it was found that nanotubes are not formed when the pH value was above 6 [31]. The different pH levels of the electrolyte lead to different current density profiles and different surface structures of TiO₂. The current densities of anodized Ti foil varied as a function of anodization time at pH 3, 5, and 7 respectively. TiO₂ nanotubes were achieved when Ti foil was anodized in fluoride solution between the low pH and neutral. The pH affected both the behavior of the electrochemical etch and chemical dissolution owing to the hydrolysis of titanium ions. The best pH range for formation of the longer nanotubes is between pH 3 and 5. However, at the lower pH the nanotubes were likely to be shorter but cleaner. For the higher pH, the longer and bigger nanotubes could be obtained [32].

The electrolytes were the first consideration factor for synthesis of TiO₂ nanotubes. TiO₂ was mainly formed by electrochemical anodization of Ti in aqueous HF and NH₄F containing electrolytes. In these electrolytes, the dissolution of TiO₂ as soluble [TiF₆]²⁻ is required for pore formation. A decade later, Grime and et al had the first studies for forming uniform titania nanotubes arrays by anodic oxidation of titanium in a hydrofluoric (HF) electrolyte by varying pH and electrolyte concentration containing acidic electrolytes [33]. Subsequently, a second method using buffered electrolytes such as solution preparation, mixing and pH adjustment was developed. The effect of electrolyte and anodization time on TiO₂ nanotubes were studied in 1 M Na₂SO₄ containing 0.3 g of NH₄F, and the results of this were nanotubes lengths ranging from approximately 0.7 to 2.5 μm with the additional aspect of altering the electrolytes pH [32]. A third method, using polar organic electrolytes such as formimide, dimethyl formimide, ethylene glycol, glycerol, HF, methanol and NH₄F was employed to fabricate TiO₂ nanotubes. Even in this organic electrolyte fluoride ions are expected to form soluble Ti fluoride complexes and therefore to dissolve the formed anodic oxide. However, due to the significant changes in the physical and chemical properties of the electrolytes, modifications in the growth behavior of the oxide layers were expected. The electrochemical behavior of fluorine containing dimethyl sulfoxide (DMSO) and ethylene glycol (EG) electrolytes and its influence in controlling the lateral dimensions of TiO₂ nanotubes were investigated [34]. In addition, TiO₂ nanotubes were grown in ammonia fluoride (NH₄F) containing organic electrolytes that synthesized the smooth tube walls several micrometers in thickness. However, as a result of the high dissolution rate the length of the nanotubes were limited within the range (200-300 nm) [35].

Self-organized TiO_2 nanotubes depend on electrolytes and pH. They also depend on voltage and anodization time parameters. The potential has an effect on the growth of TiO_2 nanotubes. The different anodic potentials show a high reproducibility of up to 40 V. During the continuous sweep phase a relatively constant current value is established and no significant irregularities occur. At every potential up to 40 V, as the potential sweep is stopped, the current density slowly decreases and levels off to an almost constant value. The final steady-state value seems to depend slightly only on the applied potential. From the samples anodized in the investigated potential range (between 2 and 40 V), the insets in the 2 and 5 V cases show detailed top-views, since the tube diameters are very small. There is a large effect of the potential on the tube diameters, ranging from 20 nm at potential 2 V, 105 nm at potential 20 V and to almost 300 nm at potential 40 V. Figure 2.5 shows an evaluation of the tube diameters and tube length dependence on the anodization potential. Within the error of the experiment, one observes a linear dependence. The layer thickness increases linearly up to about 20 V and then remains approximately constant for higher potentials. This can be ascribed to significant thinning of the tube walls due to chemical dissolution of the oxide with time [36].

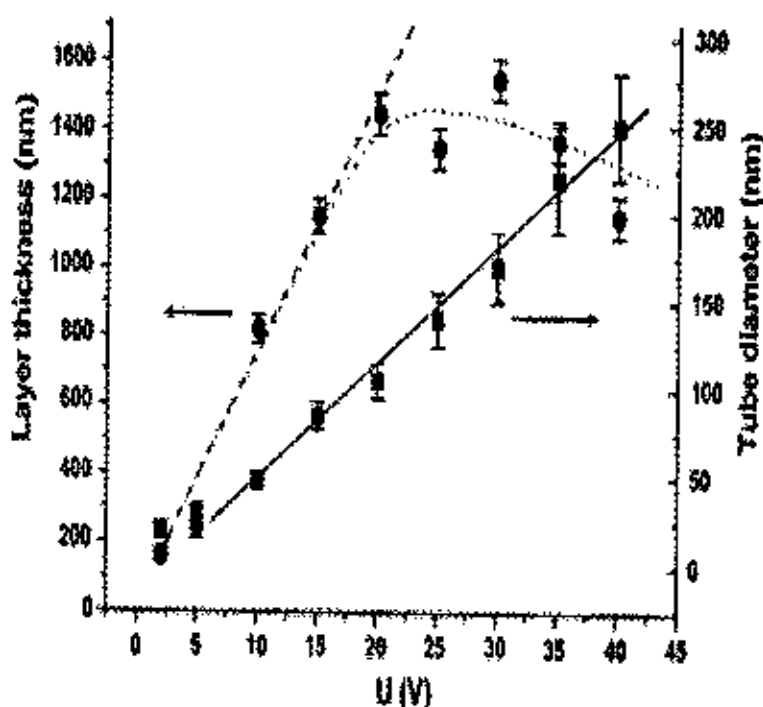


Figure 2.5 Tube diameter and thickness of the nanotubes layers [37].

Anodization time is a key parameter to consider in the growth of TiO_2 nanotubes because it offers three steps for self organization: 1) Formation of barrier layer of titanium that interacts with electrolyte when voltage was applied 2) Oxide growth and dissolution occurs and 3) There is balance of growth and chemical dissolution. Samples anodized for different times are shown in Figure 2.6. In the very first stage of the anodization, a thin and compact TiO_2 layer is formed. This layer contains some statistical distribution for breaking-down sites. For instance, accelerated dissolution occurred for locations next to the compact oxide. After 1-3 minutes, these pore nucleation events are apparent on almost the entire surface. On some locations, undermined patches of the initial compact oxide are visible. In the range of 3-10 min from the beginning of the anodization, the pores have a random appearance. In this period, pronounced dissolution at the pore bottoms takes place that makes them significantly deeper. Further, no remnant TiO_2 layer from stage 1 is present on the surface. After about 20 minutes, the porous structure starts to readily convert into a nanotubular structure. The layer thickness at this very moment is already exceeding 500 nm. By further anodization, a self-organized nanotubes layer is being fully evolved for anodization time of 1 hour. The result shows that the different TiO_2 nanotubes morphologies: at 0, 3, 10, 30 and 60 minutes formed compact TiO_2 layer, initial porous layer, initial pore growth, remaining initial porous layer, ordered tubes and self organized nanotubes layer respectively. Anodization time could be optimized for self organized TiO_2 nanotubes.

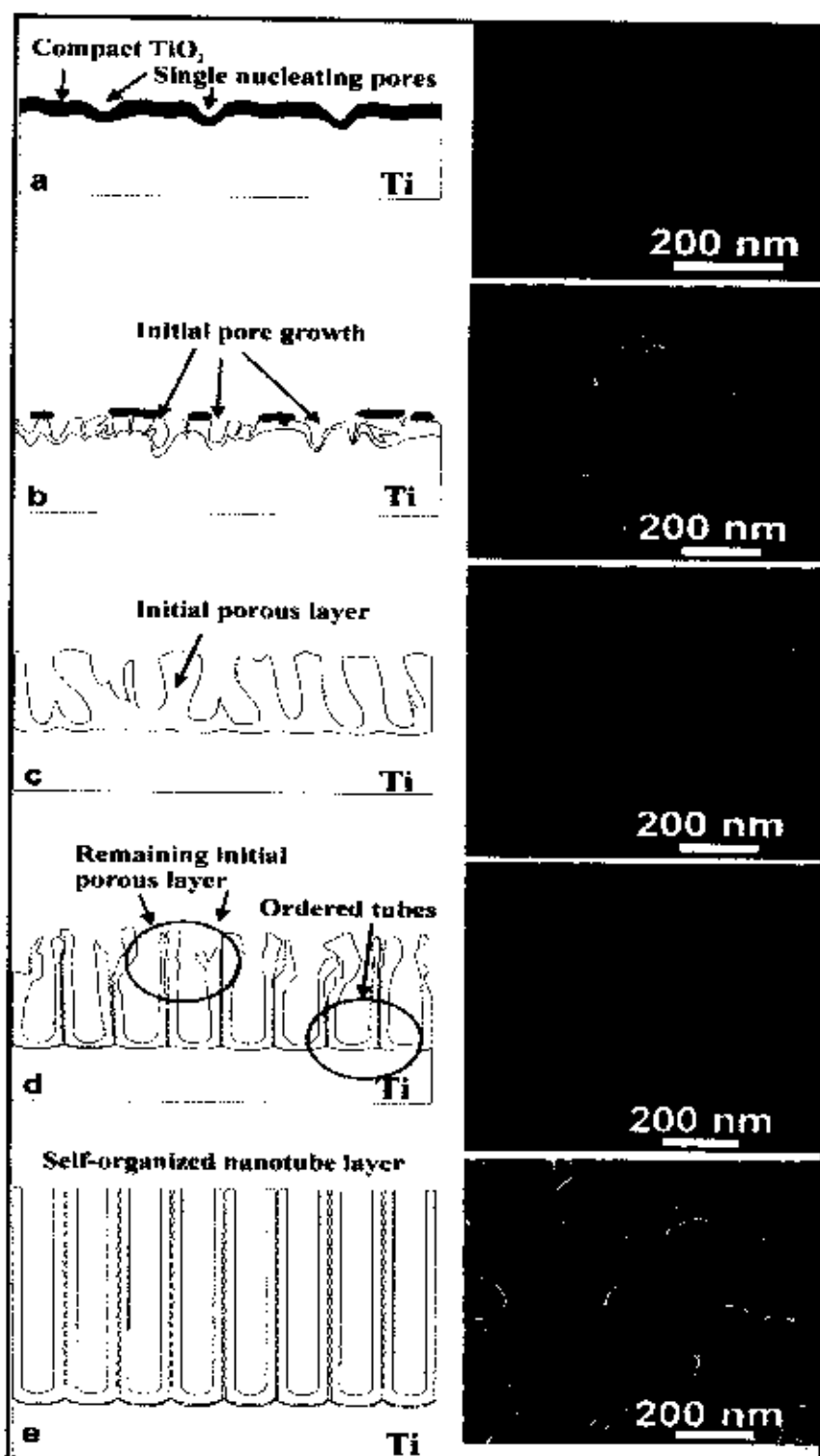


Figure 2.6 Schematical of different anodization times of the TiO_2 nanotube layer formation for (a) 0 min, (b) 3 min, (c) 10 min, (d) 30 min and (e) 1 h in water/ glycerol /0.27 M NH_4F after potential 20 V [37].

2.3 TiO₂ nanotubes formation

The anodization or anodic oxidation method is a technique for synthesizing TiO₂ nanotubes in electrolytes as an acid solution. This is done by using a small amount of hydrofluoric or fluoride ions and applying an electrical potential between a Ti foil as anode and a Pt or others metal as cathode. The formation mechanism of TiO₂ nanotubes occurs at the anode. The surface of titanium metals is even and smooth after being polished carefully. However, the surface is covered with a compact thin oxide film due to the intrinsic property of valve metal [38]. Oxide growth at the surface of the metal occurs due to interaction of the metal with O²⁻ or OH⁻ ions [39]. After the formation of an initial oxide layer, these anions migrate through the oxide layer reaching the metal/oxide interface where they react with the metal part. The compact oxide begins to dissolve and dissolution takes place only in selective area. The oxide layer formations are shown in Figure 2.7. The overall reactions for anodic oxidation of titanium can be represented as

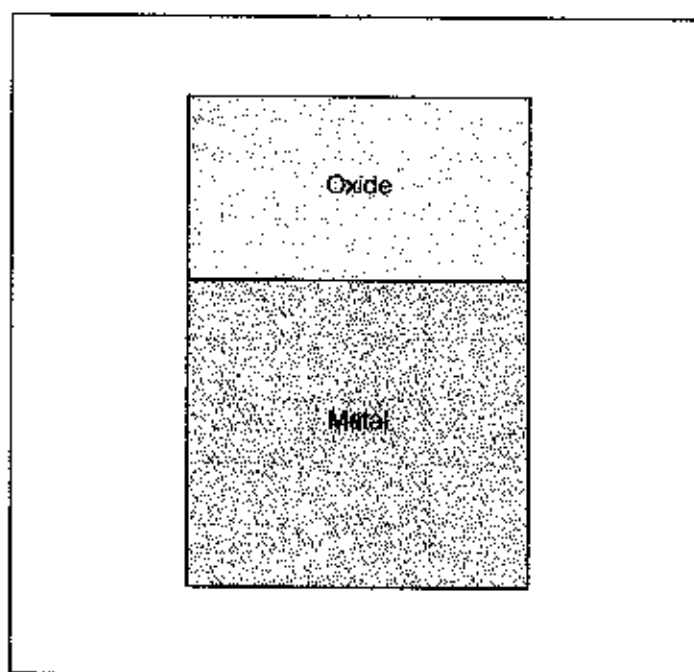
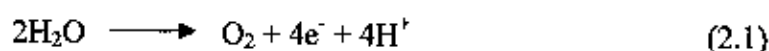


Figure 2.7 The oxide layer formations.

The compact oxide film at the titanium surface existed with or without the assistance of electric field and NH_4F solution can etch the oxide quickly. But the etching speed was different at different area of the oxide due to the different stress on the surface of oxide film which was called selective etching. Metal ion Ti^{4+} migrated from the metal/oxide interface under application of an electric field and move towards the oxide/electrolyte interface. Small pits formed due to the localized dissolution of the oxide which is shown in Figure 2.8, represented by the following reaction:

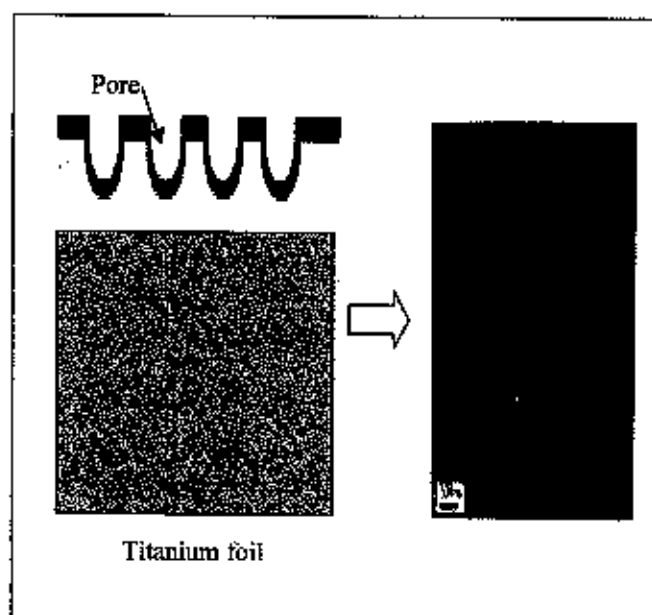
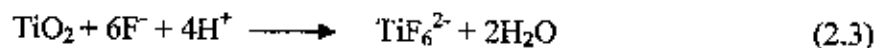


Figure 2.8 Pore formation due to fluoride addition during anodization.

Field assisted dissolution of the oxide at the oxide/electrolyte interface [40]. Due to the applied electric field the Ti-O bond undergoes polarization and is weakened, promoting dissolution of the metal cations. Ti^{4+} cations dissolve into the electrolyte, and the free O^{2-} anions migrate towards the metal/oxide interface to interact with the metal [41]. After that, the pores spread uniformly over the surface. The pore growth occurs due to the inward movement of the oxide layer at the pore bottom. Figure 2.9 shows growths of pores.

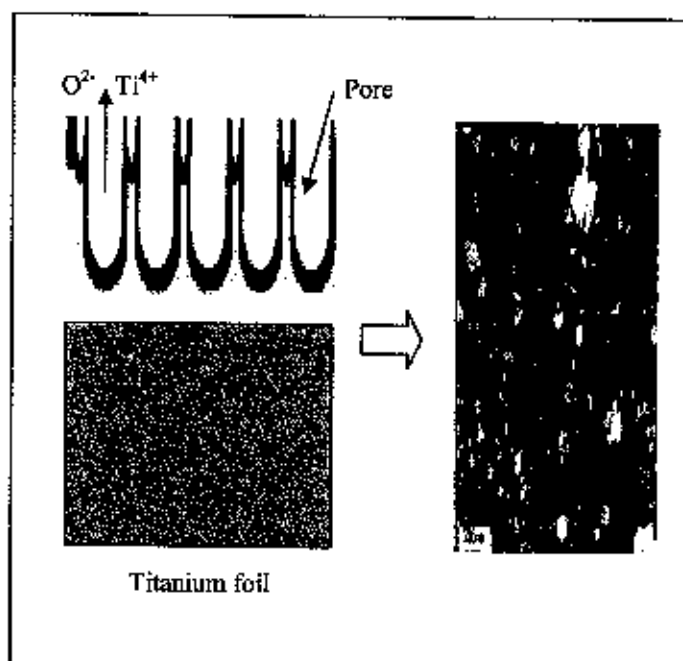


Figure 2.9 Growth of the pores due to field-assisted dissolution of titanium.

Chemical dissolution of the metal, or oxide, by the acidic electrolyte also takes place during anodization. Chemical dissolution of titania in the NH_4F electrolyte plays a key role in the formation of nanotubes rather than a nanoporous structure [42]. The rate of oxide growth at the metal/oxide interface and the rate of oxide dissolution at the pore bottom and electrolyte interface ultimately become equal; thereafter the thickness of the barrier layer remains unchanged although it moves further into the metal making the pore deeper. As the pores become deeper, the electric field in these metallic regions increases, enhancing the field-assisted oxide growth and oxide dissolution, and the interpore voids start forming as shown in Figure 2.10.

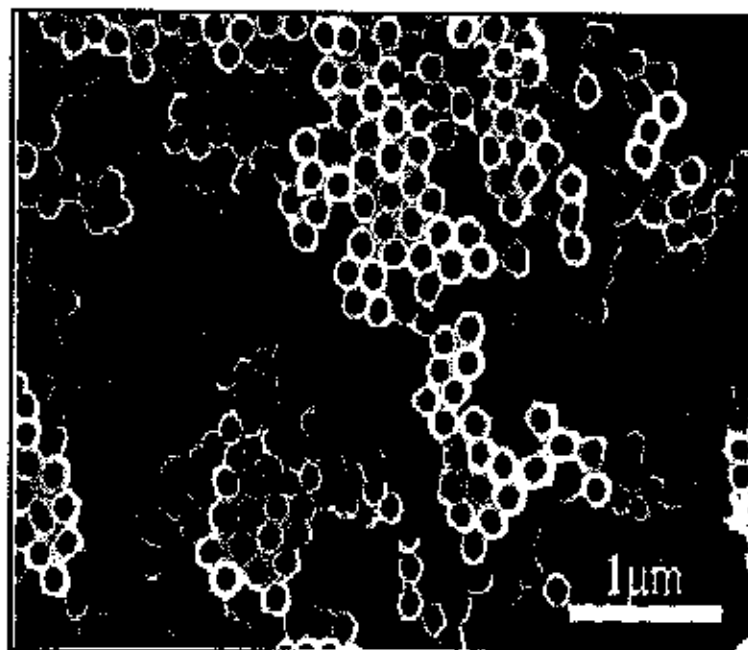


Figure 2.10 Void formation in metallic part between the pores [43].

The nanotube array is fully developed with a corresponding top view. Both voids and tubes grow in equilibrium to finally yield a tubular structure. If the titanium oxide in the wall or at the pore bottom dissolves at a balance rate, the pore depth remains constant and does not change with anodizing time. This was determined for a given electrolyte concentration and anodization potential. This chemical dissolution, the key for the self-organized formation of the nanotube arrays, reduces the thickness of the oxide layer (barrier layer) keeping the electrochemical etching (field assisted oxidation and dissolution) process active. Figure 2.11 shows formation of titania nanotubes.

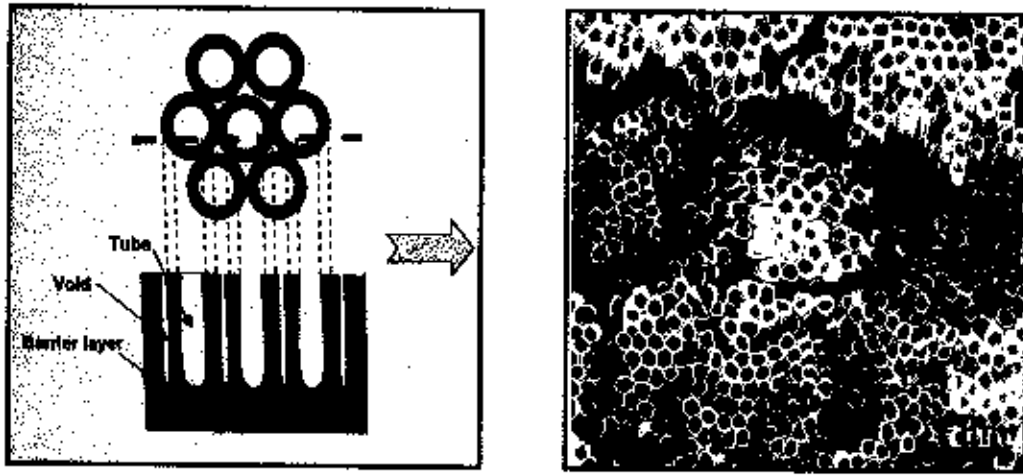


Figure 2.11 Formation of titania nanotubes.

A schematic of the electrochemical and dissolution reactions and ions path involved during anodization of titanium are presented in Figure 2.12.

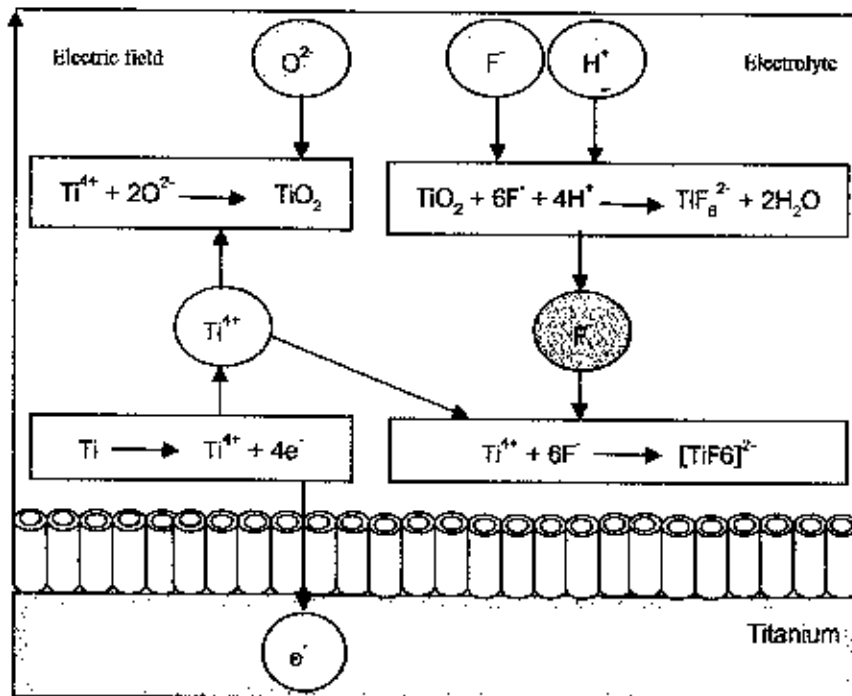


Figure 2.12 Schematic diagram of electrochemical reaction during anodization [44].

2.4 The dye-sensitized solar cells

2.4.1 Principle of dye-sensitized solar cells

Dye-sensitized solar cells are the photovoltaic devices of choice because of their high efficiency, low production cost and environmentally friendly TiO_2 semiconductor materials [45]. In general, Dye-sensitized solar cells consist of three main components: a dye-covered nanocrystalline TiO_2 layer on a transparent conducting oxide glass (TCO) substrate serving as working electrode, an iodide/triiodide redox couple. Dye-sensitization has also recently been recognized as an important process in photon harvesting from sun light, and intense scientific studies of the photon-to electron conversion of sun light using wide band gap metal oxides with ZnO , SnO_2 , TiO_2 and SrTiO_3 as semiconductors, and chlorophylls, cyanine dyes, xanthenes dyes, azo dyes and metal complexes such as ruthenium trisbipyridine complexes and Ru bipyridine as sensitizing dye. Consequently, a wide variety of dyes with differing binding groups and linkers have been tested as photosensitizer in the Gratzel cell. Anchoring to semiconductor has been achieved through a number of functional groups, such as salicylate and acetylacetonate derivatives, the most widely used and successful to date being the carboxylic acid and phosphoric acid functionalities. The carboxylic acid groups, while ensuring efficient adsorption of the dye on the surface also promote electronic coupling between the donor levels of the excited chromophore and the acceptor levels of the TiO_2 semiconductor [46].

At the heart of the system is a mesoporous oxide layer composed of nanometer-sized particles which have been sintered together to allow for electronic conduction to take place. The material of choice has been TiO_2 (anatase) although alternative wide band gap oxides such as ZnO and Nb_2O_5 have also been investigated. Attached to the surface of the nanocrystalline film is a monolayer of the charge transfer dye. A typical cell is composed of two layers of Indium tin oxide coated glass (ITO), one of which is coated with TiO_2 sand witted together with a suitable electrolyte and counter electrode. The conventional electrolyte used in this process is iodine/iodide complex and the counter electrode is simply InSnO_2 glass slide coated with a thin layer of carbon graphite. A typical setup of dye sensitized solar cell is shown in Figure 2.13.

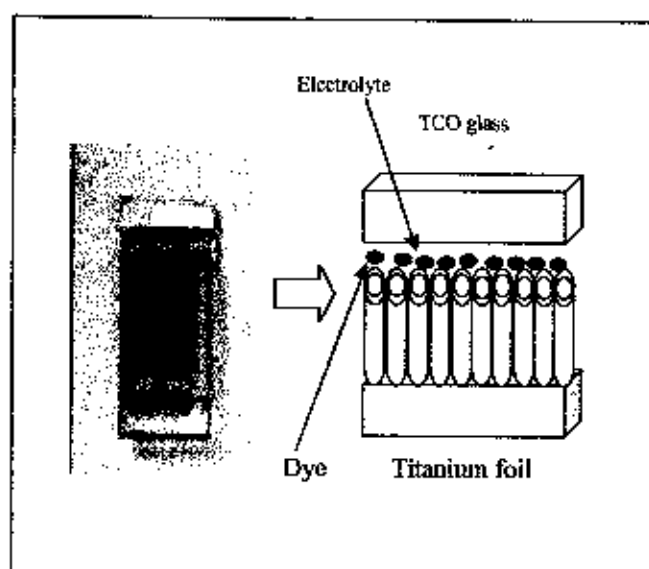


Figure 2.13 Configuration of TiO_2 nanotubes dye-sensitized solar cell.

The cell operates on a process that is similar in many respects to photosynthesis, the process by which green plants generate chemical energy from sunlight. The cell consists of a dye absorbed mesoporous metal oxide film filled with iodide/triodide redox electrolyte and Pt counter electrode. The system is a microscopic semiconductor oxide film, which is placed in contact with a redox electrolyte or an organic hole-conductor. The material of choice has been TiO_2 (anatase), although alternative wide band gap oxides such as ZnO and Nb_2O_5 have also been investigated. Attached to the surface of the nanocrystalline film is a monolayer of the sensitizer. Photoexcitation of the latter results in the injection of an electron into the conduction band of the oxide. The dye is regenerated by electron donation from the electrolyte, usually an organic solvent containing a redox system, such as the iodide/triodide couple. The regeneration of the sensitizer by iodide intercepts the recapture of the conduction band electron by the oxidized dye. The iodide is regenerated, in turn, by the reduction of triiodide at the counter electrode, with the circuit being completed via electron migration through the external load. The voltage generated under illumination corresponds to the difference between the Fermi level of the electron in the solid and the redox potential of the electrolyte. Overall, the device generates electric power from light without suffering any permanent chemical transformation [47]. The schematic presentations of the operating principles of the Dye-sensitized solar cells are given in Figure 2.14.

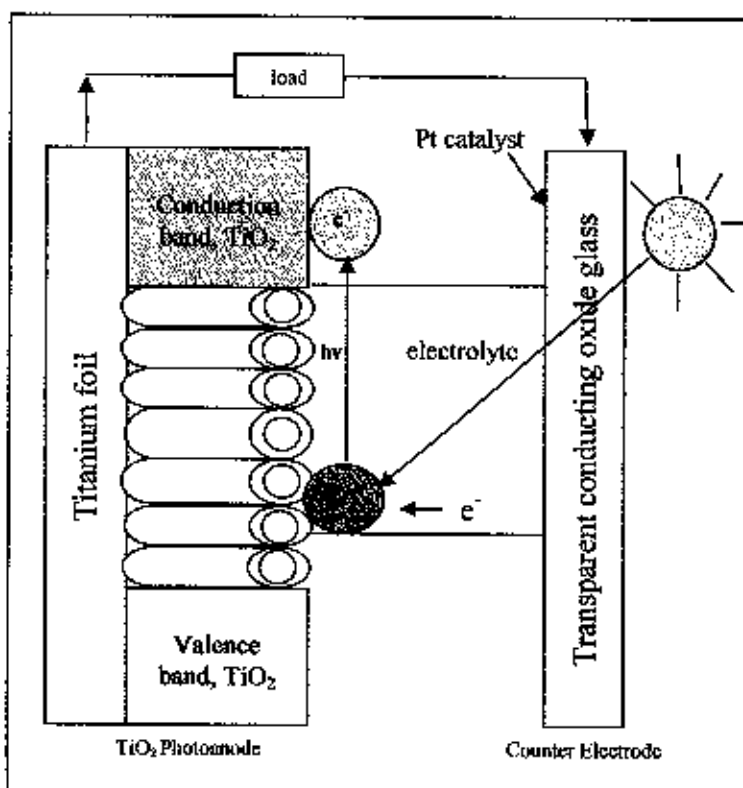


Figure 2.14 Schematic energy diagram and electron-hole transfer processes of dye-sensitized solar cells.

2.4.2 The efficiency of dye-sensitized solar cells

The current-voltage (IV) characteristics of a solar cell under illumination are used to determine the power conversion efficiency (\uparrow). Because dye sensitized solar cells have a relatively slow electrical response due to their high interfacial capacity, the voltage scan should be sufficiently slow to avoid errors in the current measurement due to capacitive discharging. After all anodization and post anodization treatment, the two TiO₂ nanotubes arrays were finally assembled into DSSCs and their IV characteristics were measured. The equations of the latter two are

$$\eta (\%) = \frac{V_{max} I_{max}}{P_{in}} \times 100 = \frac{V_{oc} I_{sc} FF}{P_{in}} \times 100 \quad (2.4)$$

$$FF = \frac{V_{max} I_{max}}{V_{oc} I_{sc}} \quad (2.5)$$

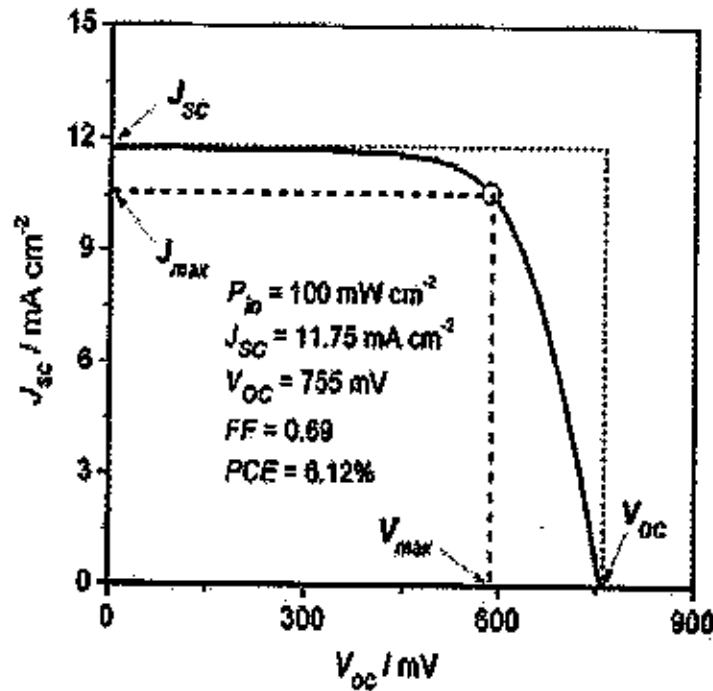


Figure 2.15 IV curve of a typical dye-sensitized solar cell [48].

Where: J_{sc} is the short-circuit current density (mA/cm^2)

V_{oc} is the open-circuit voltage (mV)

FF is fill factor

η is the conversion efficiency (%)

V_{max} is the voltage at the maximum output power (mV)

J_{max} is the current at the maximum output power (mA/cm^2)

P_{in} is the power of the incident light (mW/cm^2)

In a solar cell, power is dissipated through the resistance of the contacts and during charge transport and through leakage currents within the device or around the side of the device. These effects are electrically equivalent to resistances in series and in parallel and reduce the fill factor. Series resistance is particularly problematic at high current densities, whereas the shunt resistance is a problem in poorly rectifying devices. IV curve of typical dye-sensitized solar cell was shown in Figure 2.15.

CHAPTER 3

EXPERIMENTAL

In this chapter, the fabrication of TiO₂ nanotubes by anodization method will be described in details. First, the anodization method will be presented. Next, the characterization of TiO₂ nanotubes will be described. Third, the preparation of dye sensitized solar cells will also introduced. Finally, we describe the measurement of the efficiency of dye sensitized solar cells.

3.1 Materials and Thin films preparation

The materials used in the experiments consist of Titanium (Ti) foil (0.25 mm thickness, 99.7% purity and Sigma Aldrich), ethylene glycol (EG), ammonium fluoride (0.3 wt % NH₄F) and deionized water (2 Vol % H₂O). To clean the samples for growing TiO₂ nanotubes/Ti foils films. Next, Ti foils were cut in circular shape with diameter of 2 cm to be served as substrates. The Ti substrates were degreased ultrasonically in the solution containing isopropanol, deionized water and ethanol with duration each 10 min respectively. Finally, the samples were dried in air and used immediately in the O-ring set in the electrolyte and electrodes container. The setup is then connected with a GW laboratory DC power supply for anodization. Before the anodization, Ti substrates were mounted in a home-made housing. Only one face of the substrates was in contact with the electrolyte and was anodized. The system consisted of a two-electrode configuration with a piece of highly pure platinum counter electrode. The anode electrode was placed at the Ti foils. For, the cathode electrode is a platinum counter electrode by anidization in electrolyte.

Figure 3.2 shows experimental process of this research.

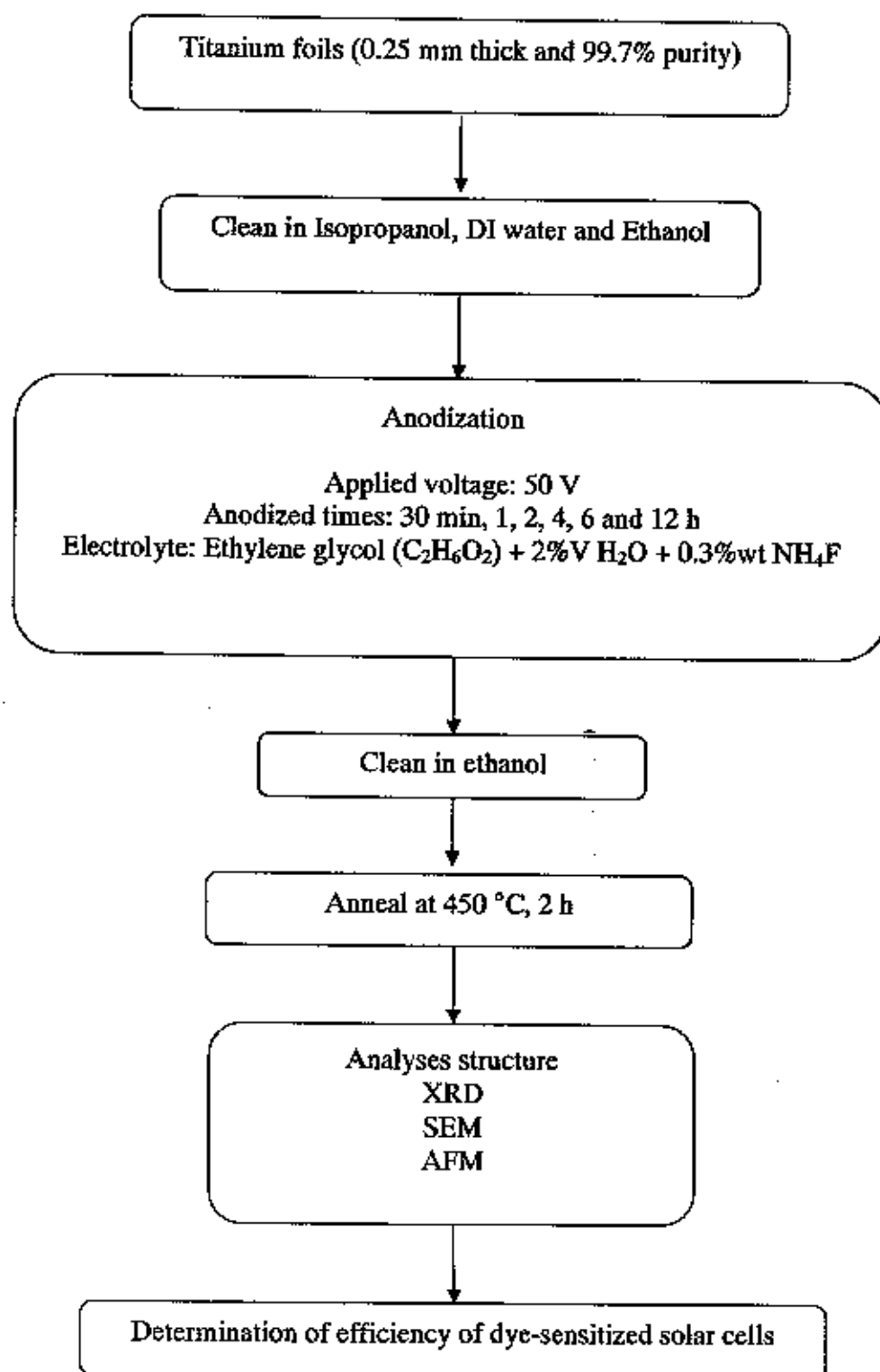


Figure 3.2 Flowchart of preparation of TiO₂ nanotubes by anodization method for dye sensitized solar cells.

3.3 The characterization of TiO₂ nanotubes

A number of analytical techniques can be employed to study the morphology and characterization of the coatings produced under different deposition conditions. However, Scanning Electron Microscopy (SEM), X-ray Diffraction (XRD) and Atomic Force Microscopy (AFM) were used in this work.

3.3.1 Scanning Electron Microscopy Analysis (SEM)

TiO₂ nanotubes morphologies were studied by Scanning Electron Microscopy. SEM analysis was carried out in a JEOL JSM-5410 Scanning Electron Microscopy with EDS attachment for quantitative elemental analysis. Figure 3.3 shows JEOL JSM-5410 Scanning Electron Microscopy.



Figure 3.3 A JEOL JSM-5410 Scanning Electron Microscopy.

3.3.2 X-ray Diffraction Analysis (XRD)

X-ray diffraction is a useful technique for orientation analysis of bulk materials and thin films. XRD analysis was performed in a PHILIPS X'Pert MPD X-RAY diffractometer using Cu K_α radiation of a wavelength of 0.154 nm is shown in Figure 3.4. The A PHILIPS X'Pert MPD can be used for normal $\theta - 2\theta$ scans, grazing incidence and high temperature scans. All three methods were employed to characterize the properties of the thin films. Scans of $\theta - 2\theta$ and high temperature scans were done at 40 kV and 30 mA. The peaks search for matching was carried out by Philips X' Pert High Score.

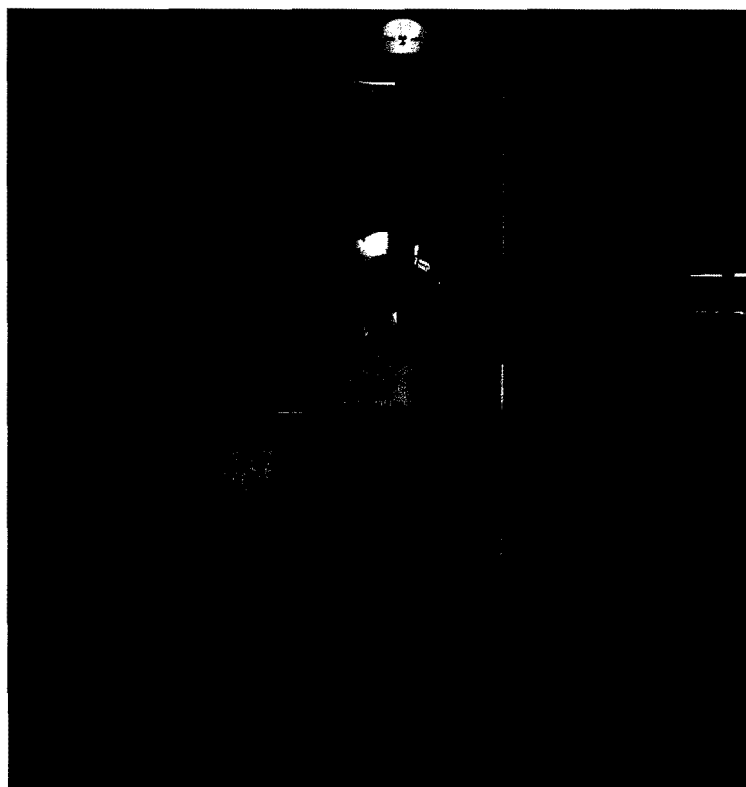


Figure 3.4 A PHILIPS X'Pert MPD diffractometer using Cu K_α radiation of a wavelength of 0.154 nm.

The degree of preferred orientation or more commonly referred to as texture was determined by normalizing the highest integrated intensity peak with the various (hkl) diffraction lines observed. Calculations of the area under the peaks, was performed using Philips PANalytical an X-ray fitting program called X' Pert Plus, developed by Philips PANalytical.

The XRD intensity profiles provide valuable information on the crystallite size. Small crystallite exhibit broad diffraction peaks. As the crystallite size increases the peak intensity becomes more intense and narrower. The crystallite size (D) is determined by measuring the full width half maximum (β) of the diffracted peak and using the Scherrer equation [49]:

$$D = \frac{k\lambda}{\beta \cos \theta} \quad (3.1)$$

Where: K is the shape factor (Scherrer constant) which is commonly equal to 0.9

β is the full width at half maximum (FWHM)

λ is the wavelength of the X-ray source (0.154 nm)

θ is the Bragg angle for the most prominent diffraction peak

The most prominent diffraction peak for this study was the (101) for Ti and other titanium. Crystallite calculations were performed using the X' Pert Plus program. It should be noted, that the X' Pert Plus program did not separate the contributions to the FWHM from crystallite size and strain. Consequently, the program can cause the crystallite sizes in the films to be slightly underestimated.

Once the Miller indices of each reflection have been determined from the XRD pattern, the lattice parameter (a, b and c) value for cubic phases for every reflection line on the XRD pattern can be calculated by employing the following equation:

$$a_0 = d_{hkl} \times \sqrt{(h^2 + k^2 + l^2)} \quad (3.2)$$

Where (hkl) are the Miller indices for the particular plane, and:

$$d_{hkl} = \frac{n\lambda}{2\sin\theta} \quad (3.3)$$

Consequently, the lattice parameter equation is:

$$a_0 = \frac{d_{hkl} \times \sqrt{(h^2 + k^2 + l^2)}}{2\sin\theta} \quad (3.4)$$

The lattice parameter values computed in this way are found to vary from one reflection to another, the variations being of two kinds, random and systematic. The random errors decrease in magnitude as the diffraction angle (θ) increases, with a striking effect as θ approaches 90° . Systemic errors manifest a definite dependence upon θ , and they also tend to a minimum as θ approaches 90° . Consequently, by plotting the lattice parameter for each reflection against $\cot\theta$ a linear fit should be obtained, with the intercept at zero corresponding to the true lattice parameter for that sample. This method is known as the “extrapolation method”.

3.3.3 Atomic Force Microscopy Analysis (AFM)

The AFM operates by scanning the surface of the coatings with a probe, which consists of a sharp tip attached to a cantilever. The movement of the cantilever tip is detected by a diode laser focused on the tip and reflected to a photodiode (Figure 3.5).

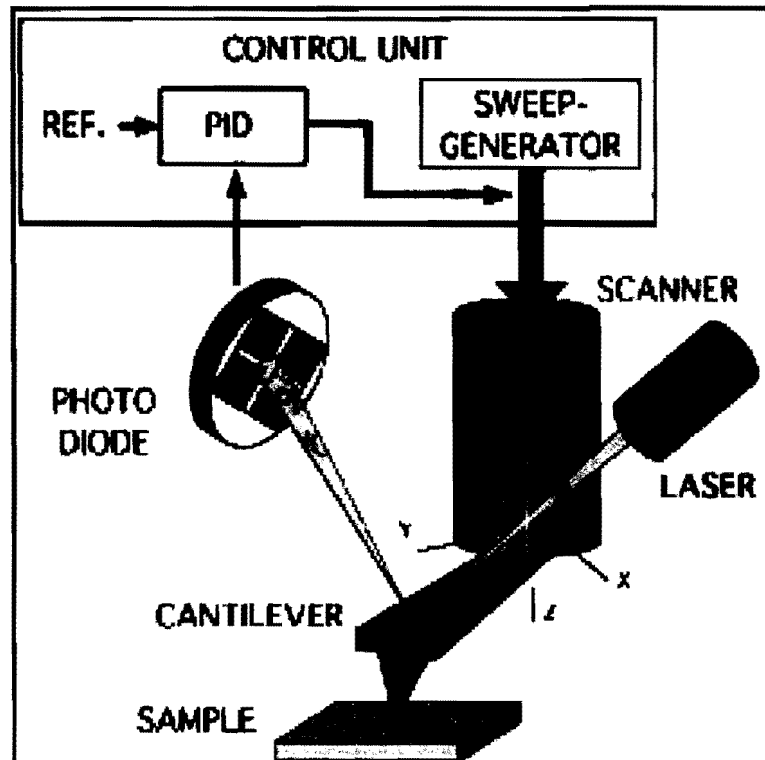


Figure 3.5 Schematic of AFM operation.

The AFM can work in two modes, namely contact and non-contact modes. In contact mode the repulsive van der Waals forces are measured between the atoms in the tip and the atoms of the materials surface. Consequently the tip is in physical contact with the surface during the analysis and can cause physical damage to soft materials. In non-contact mode the attractive van der Waals is measured by oscillating the cantilever at its resonant frequency with small amplitude some 50 to 100 angstroms from the sample surface (Figure 3.5). Because non-contact mode measures the weaker attractive forces the lateral resolution is less than that achieved with contact mode.

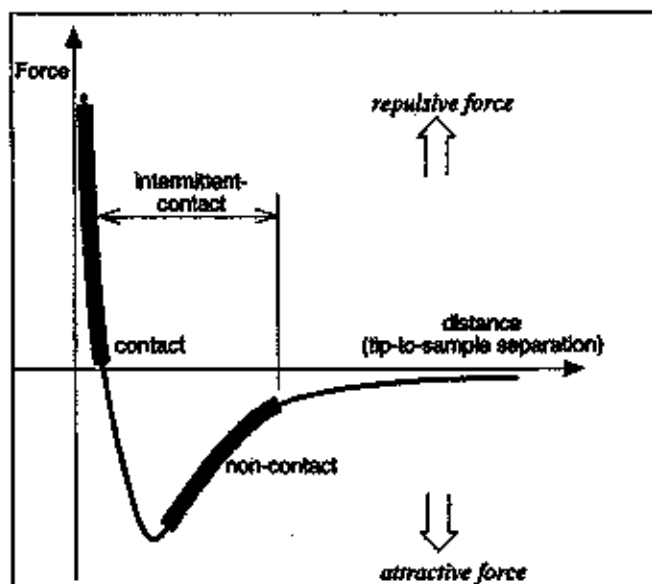


Figure 3.6 Schematic of Van der Waals force as a function of tip-sample distance in non-contact mode AFM.

A Park Scientific Instruments (PSI) "Autoprobe" Scanning Probe Microscope with an atomic force microscope (AFM) head was used to image the topography information of the coating surface in the present study. AFM analysis was performed using contact mode with ultralevers tips type C and D and 100 μm -scanner. The ultralevers tips are made from silicon and have the specifications shown in Table 3.1. Typical ultrahigh resolution AFM cantilever and conical tip is shown in Figure 3.6.

Table 3.1 Specifications of PSI "Ultralevers"

| Properties | PSI Ultralevers-Type C | PSI Ultralevers-Type D |
|--|------------------------|------------------------|
| Tip Radius (nm) | 5.0 | 5.0 |
| Force or Spring Constant (N/m) | 1.1 | 1.6 |
| Cantilever Thickness (μm) | 0.8 | 0.8 |
| Resonant Frequency (kHz) | 140.0 | 170.0 |

3.4 The preparation of dye-sensitized solar cells

TiO₂ nanotubes photoelectrode were immersed for 20 h in acetonitrile solution containing 5×10^{-4} M cis-bis (isothiocyanato) – bis (2,2' bipyridyl-4,4' dicarboxylato) ruthenium (II) bis-tetrabutyl-ammonium (N719) dye. Figure 3.7 shows immersing of N719 dye. Afterwards, the dye-sensitized TiO₂ electrodes were rinsed with ethanol and dried in air. Finally, the working electrodes were dried in an oven at temperature 80 °C 30 min.

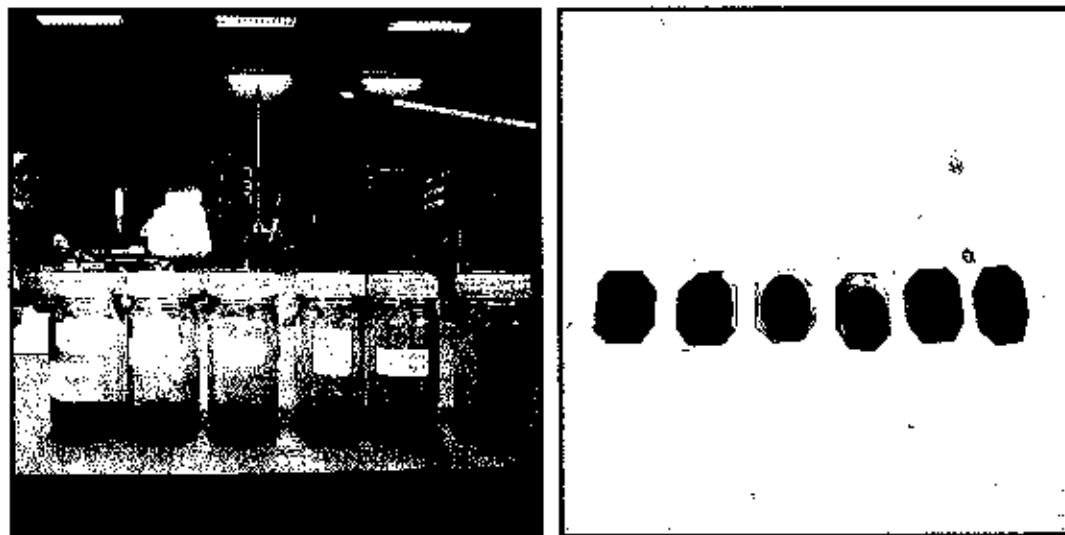


Figure 3.7 TiO₂ nanotubes were immersed in N719 dye.

A transparent conducting oxide glass (TCO) is used as counter electrode. After, TCO glass was cleaned with alcohol solution in an ultrasonic bath for 10 min and rinsed with DI water. A platinum catalyst was deposited on the TCO glass by coating with drop of platinum solution (H₂PtCl₆). The TCO glasses were heated for 30 min at 80 °C. And then, the TiO₂ nanotubes photoelectrode and Pt coated glass electrode were assembled into a sandwich. An electrolyte (KI/Iodine electrolyte) was injected into the cell. The Pt coated glass electrode was pressed on top of the working electrode to form a dye sensitized solar cell. The preparation of dye-sensitized solar cell is shown in Figure 3.8.

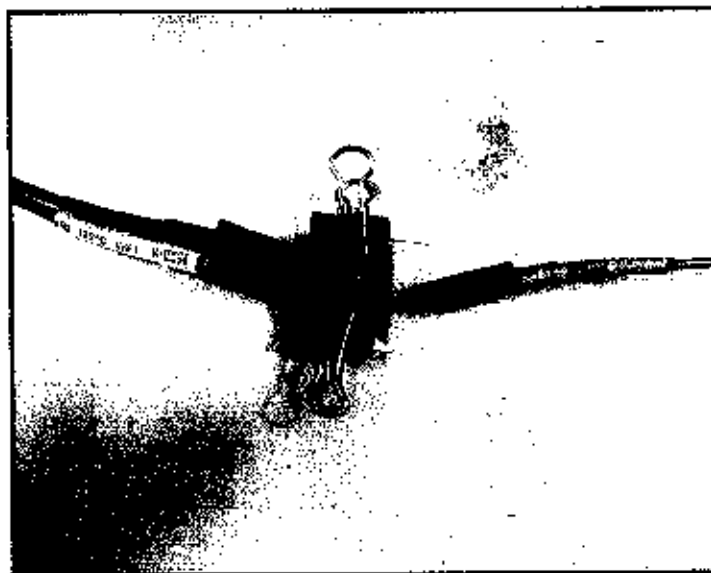


Figure 3.8 Shows preparation of dye-sensitized solar cells.

After, the light hits the working electrode. Then, the current was generated. The cells have active areas of 0.25 cm^2 . The current-voltage characteristic curves were measured with Keithley 2400 source meter. The Xenon arc lamp was used as an irradiation source and the intensity of the incident light was 70 mW/cm^2 . Measuring device of IV curves for dye-sensitized solar cells is shown in Figure 3.9. Finally, we calculated the efficiency of dye-sensitized solar cells.



Figure 3.9 Shows measurement device of IV curves for dye-sensitized solar cells.

CHAPTER 4

RESULTS AND DISCUSSIONS

The results of the morphologies, structure and efficiency of dye-sensitized solar cells of TiO_2 nanotubes will be presented in this chapter. The XRD pattern will be presented. The interpretation of XRD data will be discussed. The microstructure obtained from XRD, SEM and AFM images of TiO_2 nanotubes will be presented and discussed. Finally, the efficiency of the dye-sensitized solar cells will be presented.

4.1 XRD patterns

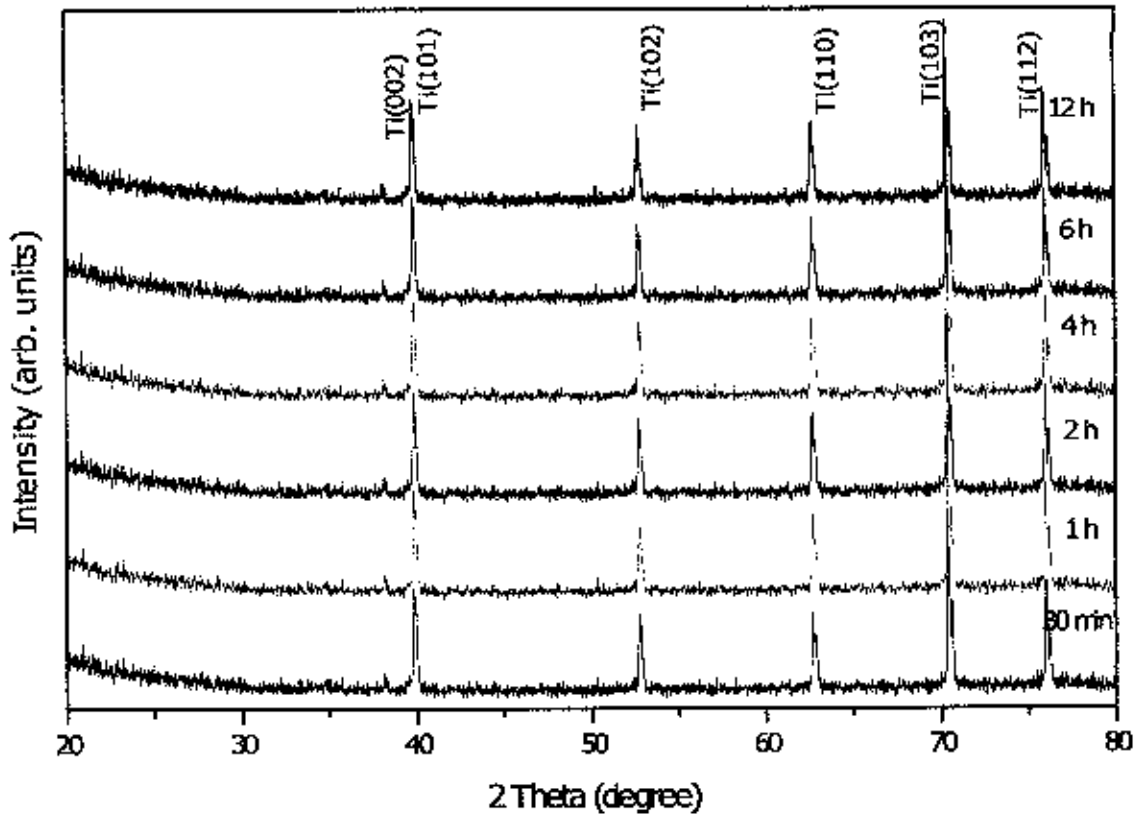


Figure 4.1 XRD patterns of the TiO_2 nanotubes as-anodized samples with different anodizing times: 30 min, 1 h, 2 h, 4 h, 6 h and 12 h before annealing.

The XRD patterns of the anodized samples without annealing were shown in Figure 4.1. The results show that all peaks belong to Ti metal sheet. The peak at $2\theta = 38.44^\circ, 40.31^\circ, 53.10^\circ, 63.05^\circ, 71.85^\circ$ and 76.63° are identified to be the (002), (101), (102), (110), (103) and (112) crystal faces respectively. The different anodizing times produce no change in the structure of pure Ti. Neither anatase nor rutile phase of TiO_2 was observed. In fact, all samples were in the amorphous phase of TiO_2 [50-51].

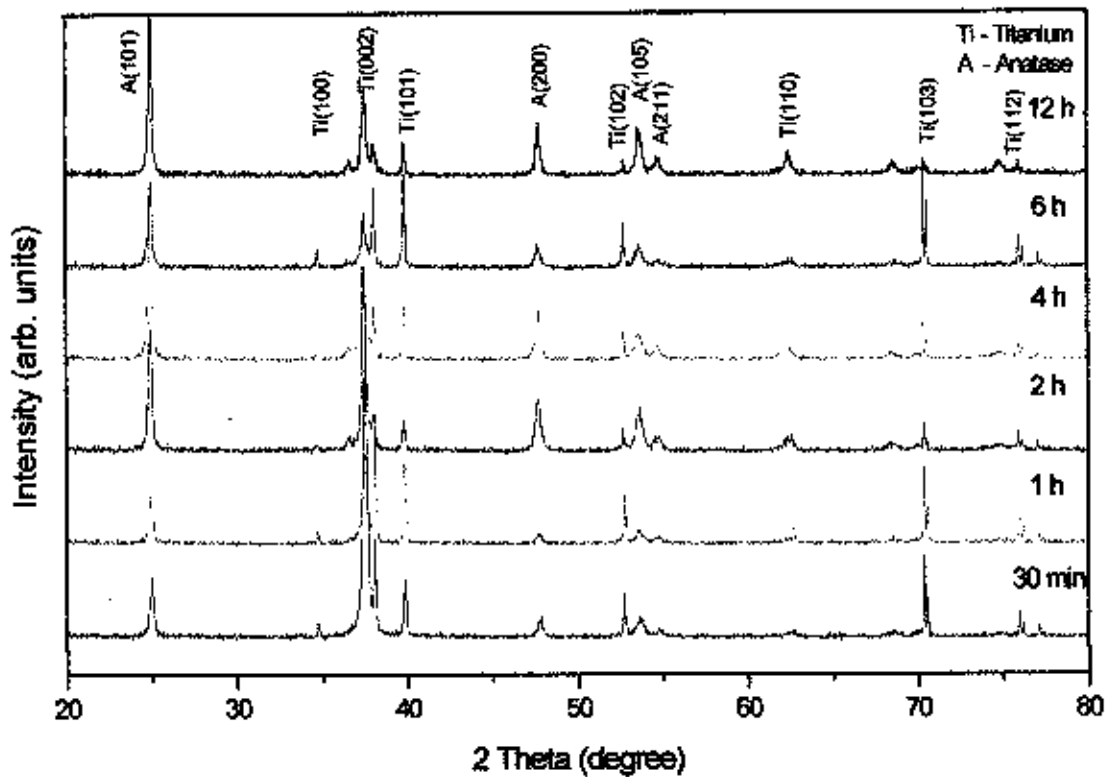
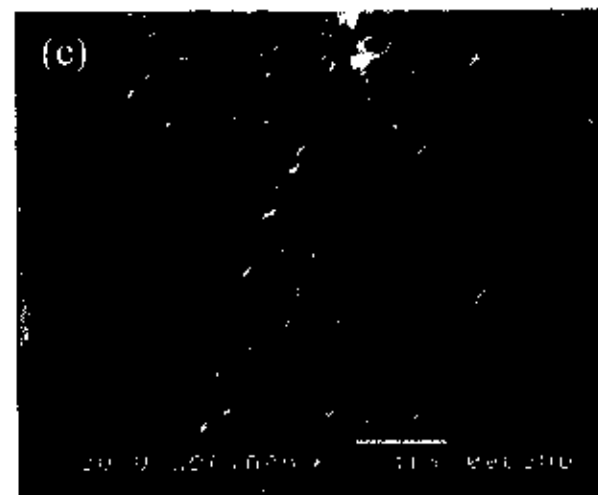
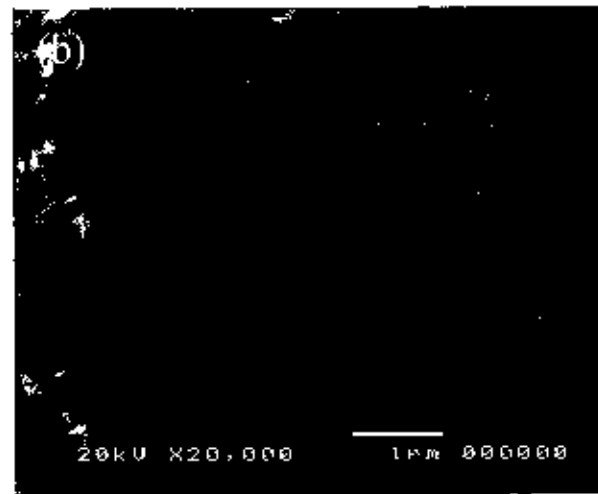
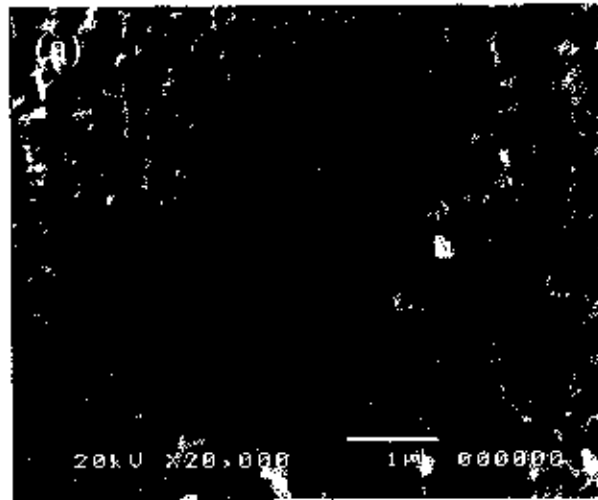


Figure 4.2 XRD patterns of the TiO_2 nanotubes with different periods of anodization: 30 min, 1 h, 2 h, 4 h, 6 h and 12 h after annealing at 450°C 2 h.

The XRD patterns of anodized samples after annealing at 450°C 2 h for different anodizing times were shown in Figure 4.2. We observed that TiO_2 transformed from an amorphous phase to a crystalline anatase phase [50]. No rutile phase was detected. This result is in agreement with the work done by Tipparach et al. [51] and Li et al. [48]. The peaks scattering angles of $25.27^\circ, 48.75^\circ, 53.46^\circ$ and 54.75° correspond to reflections from (101), (200), (105) and (211) crystalline planes of anatase TiO_2 respectively [52].

4.2 SEM analysis

The morphologies of TiO_2 nanotubes displayed in Figure 4.3 show sizes of about 30 – 220 nm for different anodizing times.



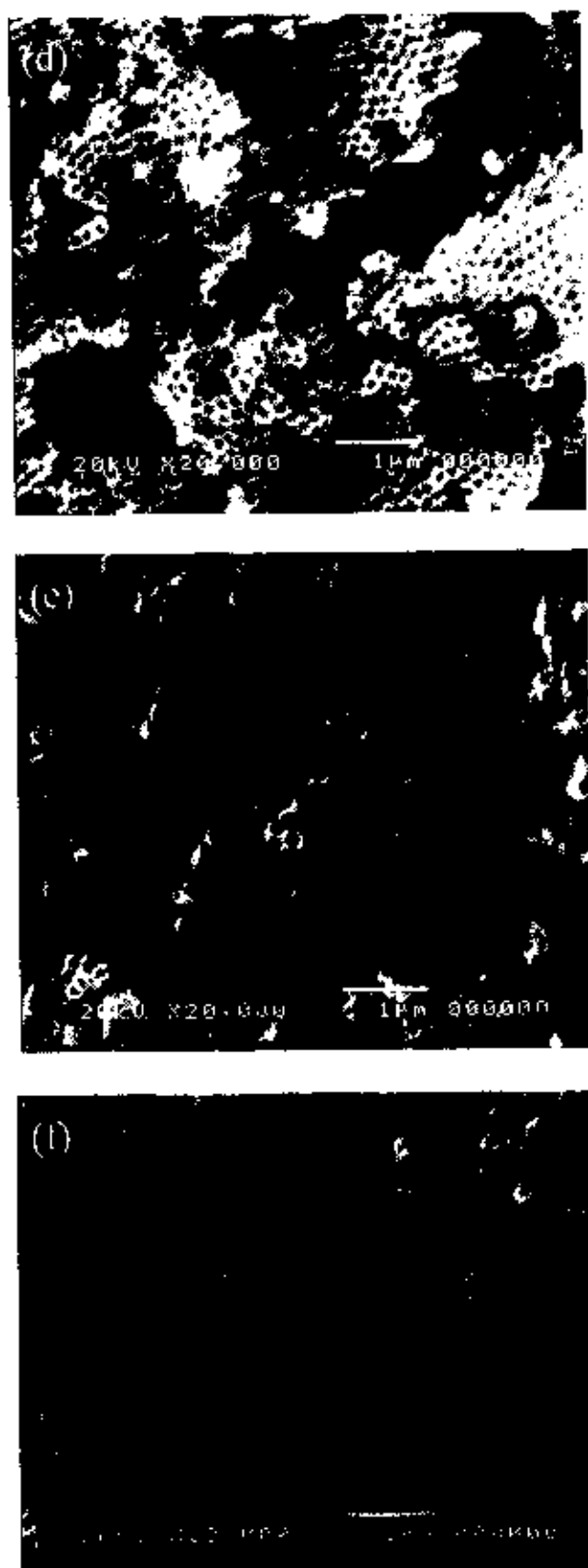
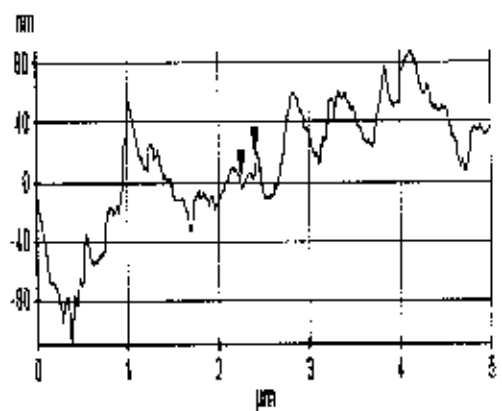
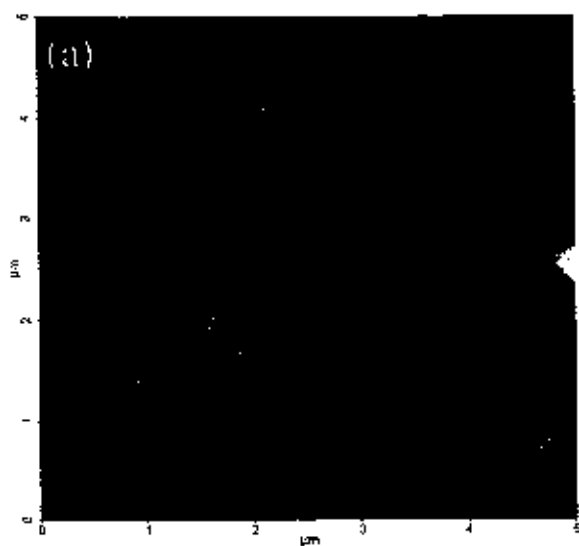


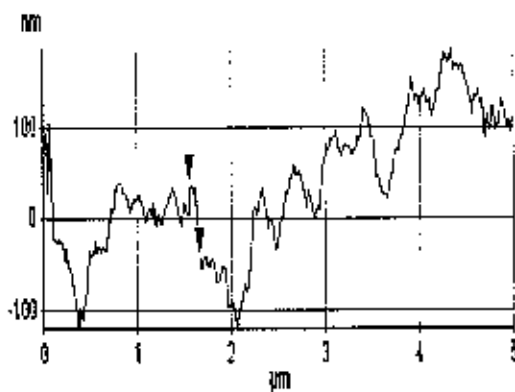
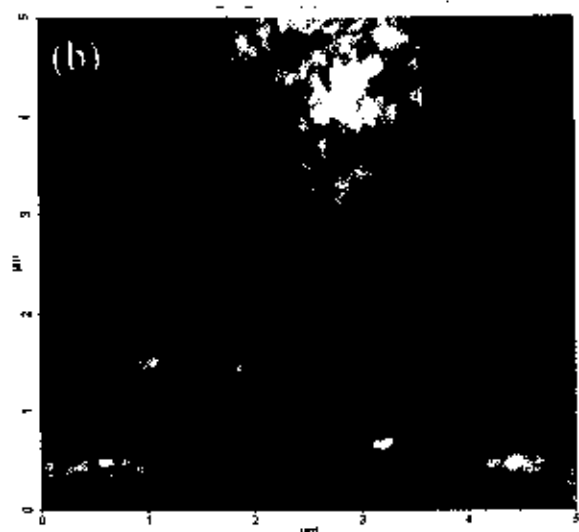
Figure 4.3 SEM images of TiO₂ nanotube arrays with different anodizing times:
(a) 30 min, (b) 1 h, (c) 2 h, (d) 4 h, (e) 6 h and (f) 12 h.

The morphology of TiO_2 nanotubes was shown in Figure 4.3 (a)-(f). The well-aligned and uniform TiO_2 nanotubes were observed for all anodizing times. It was evident that the TiO_2 nanotubes were small with diameter of about 30 nm when anodized for short periods of time 30 min for figure 4.3 (a). The size diameter of TiO_2 nanotubes are approximately 30 nm, 50 nm, 130 nm, 140 nm, 200 nm and 220 nm for anodizing times 30 min, 1 h, 2 h, 4 h, 6 h and 12 h respectively. The TiO_2 nanotubes are longer when the anodizing time was extended. From the observation, gas bubbles were observed during the anodization. In the first step, the current density between the electrodes was very high and lower when the anodizing times were extended. The gas generation slowed down as the current density decreased. The sizes of the nanotubes are similar, with a tubular structure. However, it was observed that at shorter anodizing times denser nanotubes were obtained. For longer anodizing times, dense oxide layer results in high ohmic resistance, this eventually reduces the current density. The consequence of the low current density reduces the hydrolytic ability of the electrolysis. Subsequently, this results in lowering the concentration of oxygen [53], which plays an essential role in the formation of the dense oxide layer of TiO_2 nanotubes.

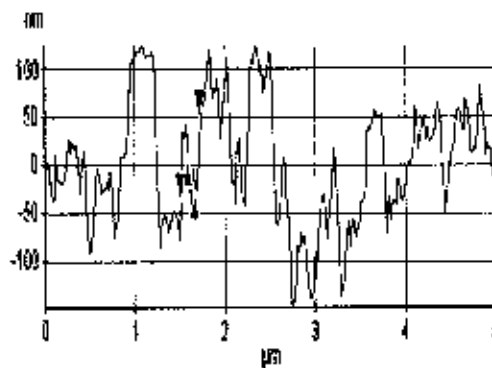
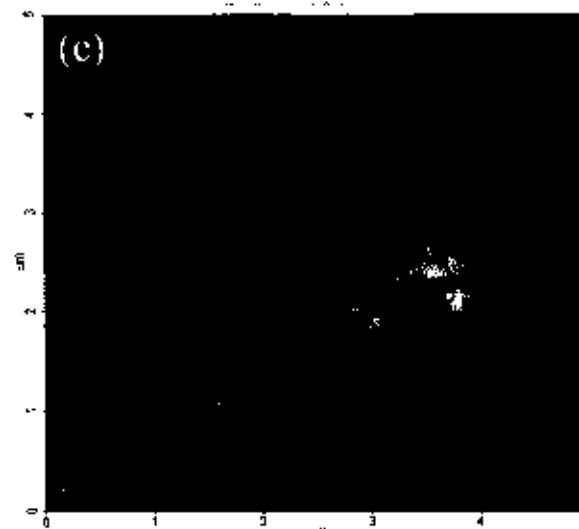
4.3 AFM analysis



| Cursor | $\Delta X(\mu\text{m})$ | $\Delta Y(\text{nm})$ | Angle(deg) |
|--------|-------------------------|-----------------------|------------|
| Red | 0.136 | 15.306 | 5.698 |



| Cursor | $\Delta X(\mu\text{m})$ | $\Delta Y(\text{nm})$ | Angle(deg) |
|--------|-------------------------|-----------------------|------------|
| Red | 0.104 | -80.571 | -37.721 |



| Cursor | $\Delta X(\mu\text{m})$ | $\Delta Y(\text{nm})$ | Angle(deg) |
|--------|-------------------------|-----------------------|------------|
| Red | 0.208 | 85.679 | 22.402 |
| Green | 0.078 | -35.479 | -24.485 |

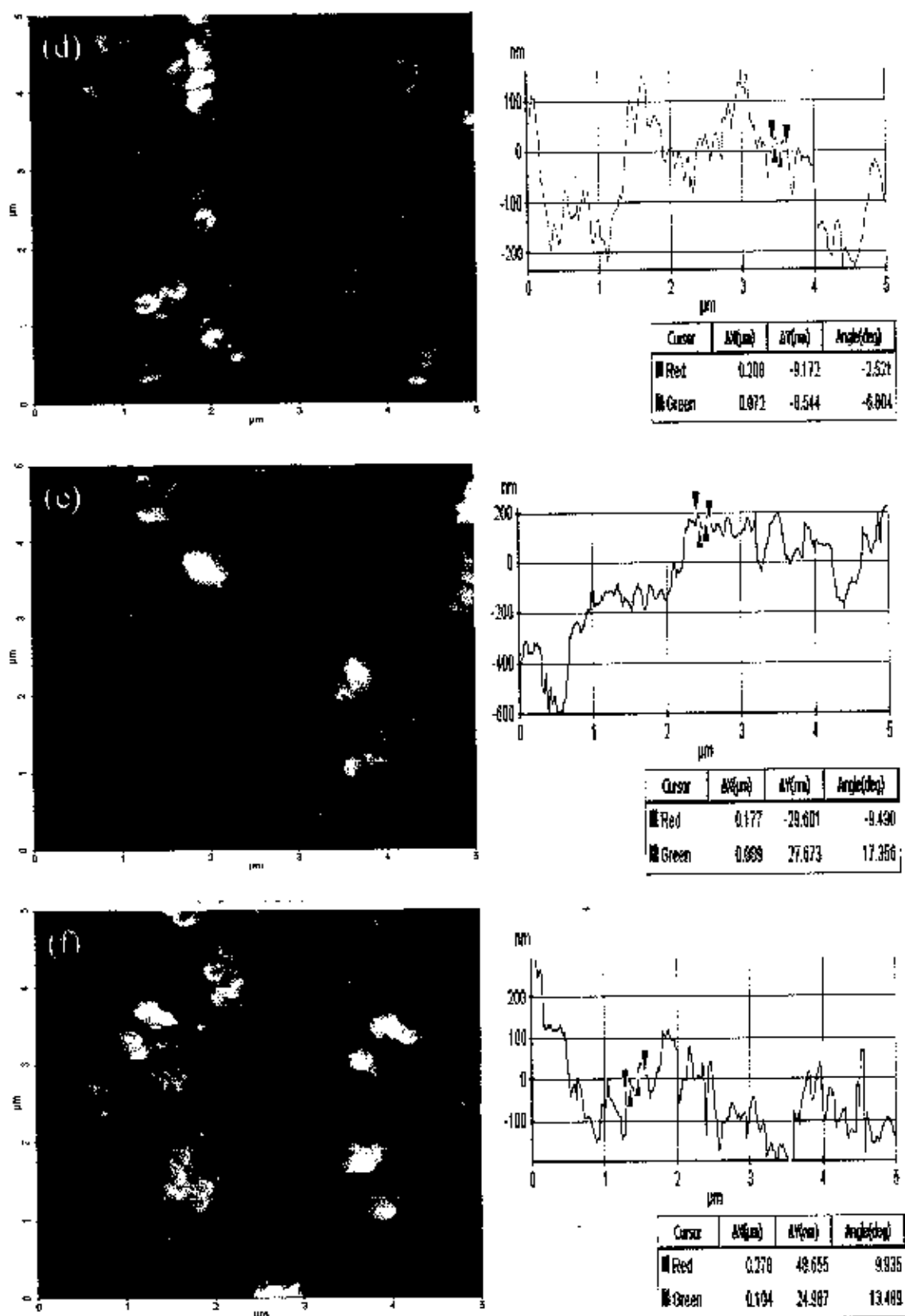


Figure 4.4 AFM images of TiO_2 nanotubes with different anodizing times: (a) 30 min, (b) 1 h, (c) 2 h, (d) 4 h, (e) 6 h and (f) 12 h.

The wall thicknesses of TiO₂ nanotubes were investigated using Atomic Force Microscope. Figure 4.4 shows Atomic Force Microscope of TiO₂ nanotube arrays with different anodizing times. The wall thickness of TiO₂ nanotubes were approximately 113 nm, 122 nm, 130 nm, 136 nm, 98 nm and 174 nm for anodizing times 30 min, 1 h, 2 h, 4 h, 6 h and 12 h respectively. The wall thickness of TiO₂ nanotubes increase with increasing the anodizing times. The wall thickness also depends on anodization parameters such as NH₄F and H₂O containing ethalene glycol. Tube diameter and the wall thickness can be tailored [54]. For longer anodizing times, the wall thickness of TiO₂ nanotubes are likely to be bigger because low current density reduces the hydrolytic ability of the electrolysis. Subsequently, this results in lower concentration of oxygen, which plays an essential role in formation of thicknesses of TiO₂ nanotubes.

4.4 The efficiencies of dye-sensitized solar cells

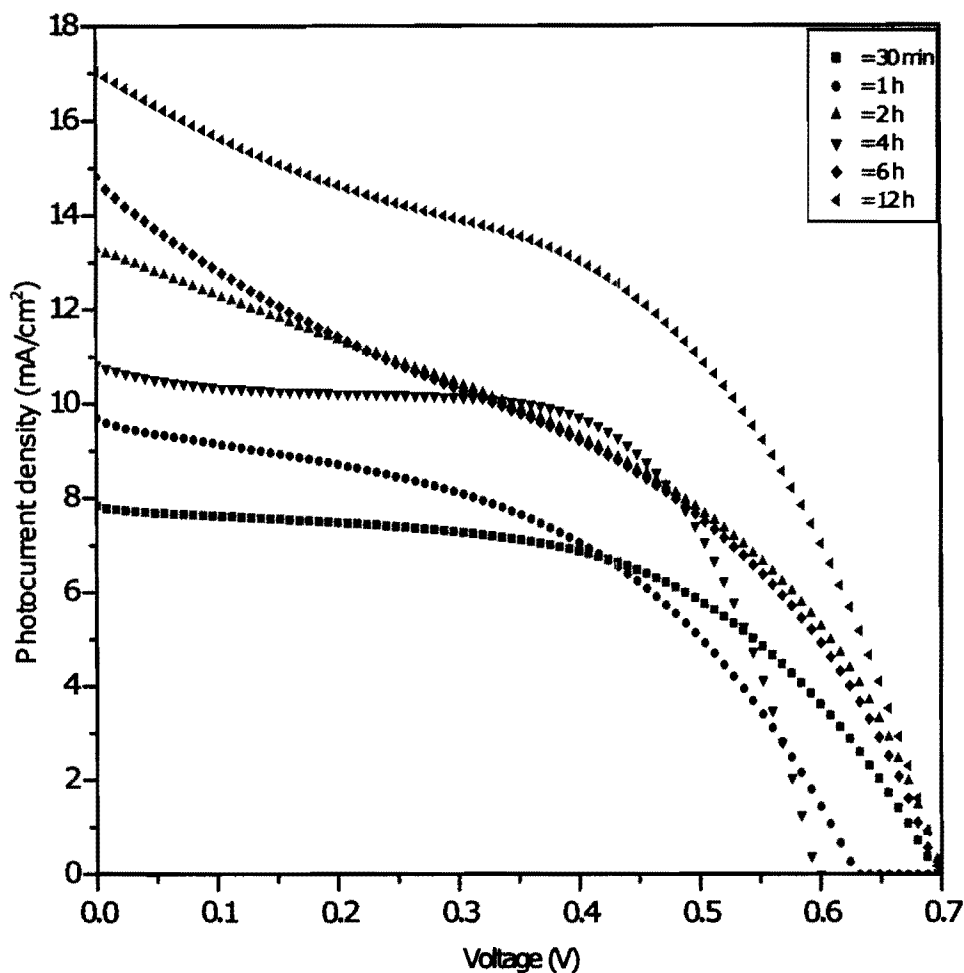


Figure 4.5 I-V characteristic of the dye-sensitized solar cells on the TiO₂ nanotube arrays with different anodizing times: 30 min, 1 h, 2 h, 4 h, 6 h and 12 h.

The efficiencies of dye-sensitized solar cells were measured by current voltage curves. The current-voltage curves were showed in Figure 4.5. The efficiencies of dye sensitized solar cells increase with increasing anodization times. Increase in anodization times will result in increase length tubes [55]. Electron transfer will be fast for longer tubes than for shorter tubes. The electrons were excited by the incident light and then injected into the conduction band of the TiO₂. The electrons diffuse rather than the electron drift that dominates the transport of the electrons from the TiO₂ to the transparent electrode in dye-sensitized solar cells [56]. As a result, the efficiencies of dye-sensitized solar cells increase with increasing the anodization times.

Table 4.1 The efficiencies of dye-sensitized solar cells.

| Anodizing times (h) | Power in (mW/cm²) | Power out maximum (mW/cm²) | Efficiency (%) |
|--------------------------------|---|--|---------------------------|
| 0.5 | 70 | 2.93 | 4.19 |
| 1.0 | 70 | 2.84 | 4.06 |
| 2.0 | 70 | 3.90 | 5.57 |
| 4.0 | 70 | 4.02 | 5.74 |
| 6.0 | 70 | 3.85 | 5.50 |
| 12.0 | 70 | 5.54 | 7.92 |

The table 4.1 shows efficiencies of dye-sensitized solar cells. When the anodization times increases from 30 min, 1 h, 2 h, 4 h, 6 h and 12 h, the efficiencies of dye-sensitized solar cells are 4.19 %, 4.06 %, 5.57 %, 5.74 %, 5.50 % and 7.92 % respectively. The efficiencies of dye-sensitized solar cells of anodizing times 4 h is 5.74 % which is more than that at 6 h because the nanotube surface after 4 h is more than that at 6 h in the figure for SEM. The electrons transfer to nanotubes at 4 h is better than at 6 h [57]. As a result, efficiencies of dye-sensitized solar cells at 4 h more than that at 6 h. The maximum efficiency for the dye-sensitized solar cell was 7.92 % for anodizing times of 12 h.

CHAPTER 5

CONCLUSIONS AND SUGGESTIONS

In this work, TiO₂ nanotubes have been synthesized by anodization in a mixture of electrolytes with different anodizing times. The TiO₂ nanotubes were used for dye-sensitized solar cells. The XRD data of as prepared samples by anodization show that all samples were amorphous even for the different anodizing times. Neither anatase nor rutile phase of TiO₂ was observed. The TiO₂ remained in their amorphous phases. After annealed, the samples were then transformed from an amorphous phase to a crystalline anatase phase.

The size of TiO₂ nanotubes is larger when the anodizing times were extended. The dense oxide layer resulted in high ohmic resistance, implying a reduction of the current density. The low current density in turn reduces the hydrolytic ability of the electrolysis. This result in low concentration of oxygen, which plays an essential role in determining the size of TiO₂ nanotubes formed. The minimum diameter of TiO₂ nanotubes was approximately 30 nm for anodizing times of 30 min. The diameter is bigger when the anodizing times increase. The wall thickness of nanotubes was observed to be greater when the anodizing times were extended. The wall thickness also depended on anodization parameters such as the electrolyte mixture of NH₄F and H₂O. The tube diameter and wall thickness can be tailored by varying anodizing times.

The efficiencies of dye-sensitized solar cells increase with increase of anodization times because the length of TiO₂ nanotubes increases with increasing anodizing times. This is a consequence of the fact that electron transfer is faster for longer tubes than for shorter tubes. The electrons were excited by the incident light and then injected into the conduction band of the TiO₂. The electrons diffuse rather than the electron drift that dominates the transport of the electrons from the TiO₂ to the transparent electrode in dye-sensitized solar cells. The maximum of efficiency for the dye-sensitized solar cell was 7.92 % for anodizing times of 12 h.

Suggestions

Future, study should be done on the electrolytic parameters. The anodizing times information may be used for controlling the size of TiO_2 nanotube arrays for synthesizing energy conversion materials such as solar cells and working electrodes for hydrogen generation by photoelectrocatalytic water splitting. In addition, TiO_2 nanotubes may be developed into heterostructures such as p-n junction and n-p-n junction for applications in electronic devices.

REFERENCES

REFERENCES

- [1] J. Zhu and M. Zach. "Nanostructured materials for photocatalytic hydrogen production", Current Opinion in Colloid & Interface Science, 14: 260-269, 2009.
- [2] V.K. Mahajan, S.K. Mohapatra and M. Misra. "Stability of TiO₂ nanotube arrays in photoelectrochemical studies", International journal of hydrogen energy, 33: 5369-5374, 2008.
- [3] H. Park and et al. "Fabrication of dye-sensitized solar cells by transplanting highly ordered TiO₂ nanotube arrays", Solar Energy Materials & Solar Cells, 95: 184-189, 2011.
- [4] M.A. Green and et al. "Solar cell efficiency tables", Prog Photovoltaics Res. Appl, 17: 320-326, 2009.
- [5] J.M. Macak, H. Tsuchiya and P. Schmuki. "High-aspect-ratio TiO₂ nanotubes by anodization of titanium", Angew. Chem. Int. Ed, 44: 2100-2102, 2005.
- [6] H. Xu and et al. "Application of ultrasonic wave to clean the surface of the TiO₂ nanotubes prepared by the electrochemical anodization", Applied Surface Science, 257: 8478-8480, 2011.
- [7] J.H. Park, S. Kim and A.J. Bard. "Novel carbon-doped TiO₂ nanotube arrays with high aspect ratios for efficient solar water splitting", Nano Lett, 6: 24-28, 2006.
- [8] O.K. Varghese and et al. "High-rate solar photocatalytic conversion of CO₂ and water vapor to hydrocarbon fuels", Nano Lett, 9: 731-737, 2009.
- [9] Y.Y. Zhang, W.Y. Fu and H.B. Yang. "Synthesis and characterization of TiO₂ nanotube for humidity sensing", Appl. Phys. Lett, 82: 281-283, 2003.
- [10] B.D. Yao and et al. "Formation mechanism of TiO₂ nanotubes", Appl Phys Lett, 82: 281-283, 2003.

REFERENCES (CONTINUED)

- [11] J.H. Jung and et al. "Creation of novel helical ribbon and double-layered nanotube TiO₂ structures using an organogel template", Chem. Mater. 14: 1445-1447, 2002.
- [12] Z.R.R. Tian and et al. "Biomimetic arrays of oriented helical ZnO nanorods and columns", J. Am. Chem. Soc. 125: 12384-12385, 2003.
- [13] H. Li and et al. "Synthesis and investigation of TiO₂ nanotubes array prepared by anodization and their photocatalytic activity", Ceramics International. 38: 5791-5797, 2012.
- [14] J.M. Macak and et al. "Smooth anodic TiO₂ nanotubes", Angewandte. Chem. International. Edition. 44(45): 7463-7465, 2005.
- [15] H. Prakasam and et al. "A new benchmark for TiO₂ nanotube arrays growth by anodization", Journal of Physical Chemistry. 111(20): 7235-7241, 2007.
- [16] G. K. Mor and et al. "Use of highly ordered TiO₂ nanotube arrays in dye sensitized solar cells", Nano Letter. 6(2): 215-218, 2006.
- [17] H. Omisvar and et al. "Influence of anodization parameters on the morphology of TiO₂ nanotubes arrays", Superlattices and Microstructures. 50: 26-29, 2011.
- [18] H. Wen and et al. "Synthesis and electrochemical properties of CeO₂ nanoparticle modified TiO₂ nanotubes arrays", Electrochimical Acta. 56: 2914-2918, 2011.
- [19] S. Dong and et al. "Rutile TiO₂ nanorod arrays directly grown on Ti foil substrates towards lithium-ion microbatteries", Thin Solid Films. 519: 5978-5982, 2011.
- [20] M. Landmann, E Rauls and W.G. Schmidt. "The electronic structure and optical response of rutile, anatase and brookite TiO₂", J. Phys. Condens. Matter. 24: 193-199, 2012.

REFERENCES (CONTINUED)

- [21] S. Bakardjieva and et al. "Photoactivity of anatase-rutile TiO₂ nanocrystalline mixtures obtained by heat treatment of homogeneously precipitated anatase", Applied Catalysis B: Environmental, 58: 193-202, 2005.
- [22] G.K. Mor and et al. "A review on highly ordered, vertically oriented TiO₂ nanotube arrays: fabrication material properties and solar energy applications", Solar Energy Material & Solar Cells, 90(14): 2011-2075, 2006.
- [23] C. A. Grimes and G. K. Mor. "TiO₂ nanotubes arrays: synthesis, properties and application", Springer, 156-158, 2007.
- [24] A. G .S. Prado and et al. "Nb₂O₅ as efficient and recyclable photocatalyst for indigo carmine degradation", Applied Catalysis B: Environmental, 80(3): 219-224, 2008.
- [25] A Fujishima and K. Honda. "Electrochemical photolysis of water at a semiconductor electrode", Nature, 238: 37-38, 1972.
- [26] O.K. Varghese and et al. "High-rate solar photocatalytic conversion of CO₂ and water vapour to hydrocarbon fuels", Nano Lett. 9: 731-737, 2009.
- [27] J.H. Park, S. Kim and A.J. Bard. "Novel carbon-doped TiO₂ nanotube arrays with high aspect ratios for efficient solar water splitting", Nano Lett. 6: 24-28, 2006.
- [28] O.K. Varghese and et al. "High-rate solar photocatalytic conversion of CO₂ and water vapour to hydrocarbon fuels", Nano Lett. 9: 731-737, 2009.
- [29] Y.S. Chen, J.C. Crittenden and S. Hackney. "Preparation of a novel TiO₂ based p-n junction nanotube photocatalyst", Environ. Sci. Technol., 39: 1201-1208, 2005.
- [30] S. Yuan, Y. Chen and Y. Zhang. Chem. React. Eng. Technol. 24: 147, 2008.
- [31] X. Feng, J.M. Macak and P. Schmuki. Chem. Mater. 19: 1534-1539, 2007.
- [32] S. Sreekantan and et al. "Influence of electrolyte pH on TiO₂ nanotube formation by Ti anodization", Journal of Alloy and Compounds, 485(1-2): 478-483, 2009.

REFERENCES (CONTINUED)

- [33] D. Gong and et al. "Titanium oxide nanotube arrays prepared by anodic oxidation", Journal of Materials Research, 16: 3331-3334, 2001.
- [34] V.C. Anitha and et al. "Electrochemical tuning of titania nanotube morphology in inhibitor electrolytes", Electrochimica Acta, 55(11): 3703-3713, 2010.
- [35] S. Sreekanta and et al. "Influence of electrolyte pH on TiO₂ nanotube formation by Ti anodization", Journal of alloys and compounds, 485:478-483, 2009.
- [36] K. Yasuda and P. Schmuki. Electrochim. Acta, 52:4053, 2007.
- [37] J.M. Macak and et al. "Mechanistic aspects and growth of large diameter self organized TiO₂ nanotubes", Journal of Electrochemistry, 621(2): 254-266, 2008.
- [38] J. Choi and M. Whan. "Anodization of nanoimprinted titanium: a comparison with formation of porous alumina", Electrochimica Acta, 49: 2645-2652, 2004.
- [39] O.K. Varghese and et al. "A titania nanotube array room temperature sensors for selective detection of hydrogen at low concentrations", Journal of nanoscience and nanotechnology, 4(7): 733-737, 2004.
- [40] D.D. Macdonald. "The formation of voids in anodic oxide films on aluminum", Journal of Electrochemistry Society, 140: L27-L30, 1993.
- [41] J. Siejka and C. Ortega. "Study of field assisted pore formation in compact anodic oxide films on aluminum", Journal of Electrochemistry Society: Solid State Science Technology, 124: 883-891, 1997.

REFERENCES (CONTINUED)

- [42] H. Wu, X. Zhang and K.R. Hebert. "Atomic force microscopy study of the initial stages of anodic oxidation of aluminum in phosphoric acid solution", Journal of Electrochemistry Society, 147:2126-2129, 2000.
- [43] S. Chen and et al. "Study on titania nanotube arrays prepared by titanium anodization in $\text{NH}_4\text{F}/\text{H}_2\text{SO}_4$ solution", Journal of Photochemistry and Photobiology, 177:177-180, 2006.
- [44] T.W. Lui. Preparation of TiO_2 photoanode and application in hydrogen generation via electrochemical process. Doctor's of thesis. Taiwan: National Cheng kung University, 2006.
- [45] U. Bach and et al. "Solid state dye-sensitized mesoporous TiO_2 solar cells with high photon to electron conversion efficiencies", Nature, 395(6702): 583-585, 1998.
- [46] W.M. Campbell and et al. "Review porphyrins as light harvesters in the dye sensitized TiO_2 solar cell", Coordination Chemistry Reviews, 248: 1363-1379, 2004.
- [47] M. Gratzel. "Review dye-sensitized solar cell", Journal of Photochemistry and Photobiology C, 4: 145-153, 2003.
- [48] S. Li and et al. "The role of the TiO_2 nanotubes array morphologies in the dye sensitized solar cells", Thin Solid Films, 520: 689-693, 2011.
- [49] A.W. Burton and et al. "On the estimation of average crystallite size of zeolites from the Scherrer equation: A critical evaluation of its application to zeolites with one-dimensional pore systems", Microporous and Mesoporous Materials, 117: 75-90, 2009.
- [50] S G. Liu, N. Hoivik and K. Wang. "Small diameter TiO_2 nanotubes with enhanced photoresponsivity", Electrochemistry Communications, 28: 107-110, 2013.

REFERENCES (CONTINUED)

- [51] U. Tipparach and et al. "Preparation and characterization of nano-TiO₂ thin films by sol-gel dip-coating method", J. Nat. Sci. Special Issue on Nanotechnology, 7(1): 129-136, 2008.
- [52] Z. He, and et al. "Electrochemical behavior and photocatalytic performance of nitrogen-doped TiO₂ nanotube arrays powders prepared by combining anodization with solvothermal process", Ceramics International, 39: 5545-5552, 2013.
- [53] J. Gong, Y. Lai and C. Lin. "Electrochemically multi-anodized TiO₂ nanotube arrays for enhancing hydrogen generation by photoelectrocatalytic water splitting", Electrochimica Acta, 55: 4776-4782, 2010.
- [54] V. Galstyan and et al. "Fabrication of pure and Nb-TiO₂ nanotubes and their functional properties", Journal of Alloys and Compounds, 536S: S488-S490, 2012.
- [55] R. Liu and et al. "Fabrication of TiO₂ nanotube arrays by electrochemical anodization in an NH₄F/H₃PO₄ electrolyte", Thin Solid Films, 519: 6459-6466, 2011.
- [56] F. Pichot and B.A. Gregg. "The Photovoltage-Determining Mechanism in Dye-Sensitized Solar Cells", Journal Physics Chemistry B, 104(1): 6-10, 2000.
- [57] H. Park and et al. "Fabrication of dye-sensitized solar cells by transplanting highly ordered TiO₂ nanotube arrays", Solar Energy Materials & Solar Cells, 95: 184-189, 2011.

APPENDIX

PUBLICATIONS/PROCEEDINGS

PUBLICATIONS

1. **B. Samran**, P. Krongkitsiri, S. Pimmongkol, S. Budngam and U. Tipparach, "Preparation and Microstructure of Titania (TiO₂) Nanotube Arrays by Anodization Method", *Advance Materials Research*, Volume 802, 2013, Pages 104-108.
2. **B. Samran** and U. Tipparach. "Structure and Electrical Resistivity of PrBa₂(Cu_{1-x}M_x)O₇", *THAJOURNAL OF PHYSICS, SERIES 8*, 2012, Pages 29-32.
3. S. Wantawee, P. Krongkitsiri, T. Saipin, **B. Samran** and U. Tipparach. "Synthesis and Structure of Titania Nanotubes for Hydrogen Generation", *Advance Materials Research*, Volume 741, 2013, Pages 84-89.

PROCEEDINGS

1. **B. Samran**, P. Krongkitsiri, T. Saipin, S. Wantawee, S. Budngam and U. Tipparach. "Fabrication and Characterization anodized Titania Nanotubes for enhancing hydrogen generation", *Proceedings of the 8th Annual conference of Thai Physics Society, SPC 2013: Organized by Chiang Mai, Thailand*, Pages 255-258.